

Linear optical properties of solids within the full-potential linearized augmented planewave method

C. Ambrosch-Draxl¹ and J. O. Sofo^{1,2}

¹*Institut für Theoretische Physik, Universität Graz,
Universitätsplatz 5, A-8010 Austria*

²*Department of Physics and Materials Research Institute,
The Pennsylvania State University,
104 Davey Lab. PMB#172, University Park PA 16802, USA*

(Dated: October 23, 2018)

Abstract

We present a scheme for the calculation of linear optical properties by the all-electron full-potential linearized augmented planewave (LAPW) method. A summary of the theoretical background for the derivation of the dielectric tensor within the random-phase approximation is provided together with symmetry considerations and the relation between the optical constants. The momentum matrix elements are evaluated in detail for the LAPW basis, and the interband as well as the intraband contributions to the dielectric tensor are given. Results are presented for the metals aluminum and gold, where we crosscheck our results by sumrules. We find that the optical spectra can be extremely sensitive to the Brillouin zone sampling. For gold, the influence of relativistic effects on the dielectric function is investigated. It is shown that the scalar-relativistic effect is much more important than spin-orbit coupling. The interpretability of the Kohn-Sham eigenstates in terms of excited states is discussed.

I. INTRODUCTION

Optical properties of solids are a major topic, both, in basic research as well as for industrial applications. While for the former origin and nature of different excitation processes is of fundamental interest, the latter can make use of them in many opto-electronic devices. These wide interests require experiment and theory to go hand in hand, and thus asks for reliable theoretical concepts.

In solid state theory, the most successful method for the calculation of materials properties is density functional theory (DFT). Lattice properties like equilibrium volumes and lattice parameters, atomic positions, phonon frequencies and elastic constants differ from their experimental counterparts by a few percent only. While, however, such ground state (GS) properties, which are based on the calculation of the total energy, are described very reliably, the treatment of excited states is not rigorously justified. The main reasons are that the Hohenberg-Kohn¹ theorem is exact only for the GS, and that the Kohn-Sham eigenstates² should not be interpreted as single-electron states. Moreover, approximations have to be made also in the ground state calculations for describing exchange and correlation effects. As a consequence, the band gap problem for semiconductors is one of the most intriguing problems in the field.

Nevertheless the interpretation of the KS states in terms of excited states has been successful for a variety of materials. Moreover, it has been claimed that the KS wavefunctions hardly differ from the many-body wavefunctions.^{3,4} It has to be pointed out that the calculation of optical properties does not go beyond the interpretation of KS eigenvalues in terms of the band structure. In this context, it may be hard to distinguish whether the shortcomings are due to the over-interpretation of GS properties or to the approximations used to solve the KS equations, e.g. the local density approximation (LDA). To gain more insight, a series of results is needed where no further approximations are introduced when solving the KS equations.

To this extent we have chosen the full potential linearized augmented planewave (LAPW) method where no shape approximation for the potential is made. We have developed the formalism of treating optical properties within the random phase approximation (RPA) taking into account inter- as well as intraband contributions. In terms of applications we focus on metallic cases for the following reasons. (i) Metals don't suffer from the band gap

problem; (ii) metals are quite well described by the LDA, and (iii) the RPA is justified due to the effective screening.

The paper is organized as follows: In Section II, the optical response within the RPA is discussed, where a short comparison to time-dependent density functional theory (TDDFT) is made. Symmetry considerations, and the description of other optical constants obtained via the Kramers–Kronig relations follow hereafter. Section III is dedicated to the treatment of the optical response within the LAPW method. First, the basic definitions of the needed quantities, are given, then the momentum matrix elements are derived within the LAPW basis. The next section contains results obtained for the elemental metals aluminum and gold. Finally, conclusions are drawn on our results for the two metallic cases. The extension of the method with localized basis functions (local orbitals) is described in the Appendix together with some mathematical relations which are useful in the derivation of the formulas.

II. THEORETICAL BACKGROUND

A. Optical response

The optical properties of solids are given by the response of the electron system to a time-dependent electromagnetic perturbation caused by the incoming light. As such, the calculation of these properties is reduced to the calculation of a response function that is the complex dielectric tensor or equivalently the polarizability. An exact expression for it is of course not known and one has to resort to the usual techniques of many-body perturbation theory to derive approximations. The first of these is the RPA.

A particular case of the general expression for the dielectric function in the RPA is the well known Lindhard formula,⁵

$$\epsilon(\mathbf{q}, \omega) = 1 + \frac{2v(\mathbf{q})}{\Omega_c} \sum_{\mathbf{k}} \frac{f_0(\varepsilon_{\mathbf{k}+\mathbf{q}}) - f_0(\varepsilon_{\mathbf{k}})}{\varepsilon_{\mathbf{k}+\mathbf{q}} - \varepsilon_{\mathbf{k}} - \omega}, \quad (2.1)$$

where

$$v(\mathbf{q}) = \frac{4\pi e^2}{|\mathbf{q}|^2} \quad (2.2)$$

is the Coulomb interaction, Ω_c the unit cell volume, f_0 the Fermi distribution function, and $\varepsilon_{\mathbf{k}}$ the single particle energy. The factor 2 comes from the summation over the spin. This corresponds to a free electron gas in the Hartree approximation, namely, the electron-electron

interaction is reduced to the interaction of each electron with a homogeneous self-consistent field. Many equivalent ways of deriving this expression have been given in the literature.^{6,7}

According to Hedin⁸ the dielectric function is defined as

$$\epsilon(\mathbf{r}, t; \mathbf{r}', t') = \delta(\mathbf{r} - \mathbf{r}')\delta(t - t') - \int P(\mathbf{r}, t; \mathbf{r}'', t')v(\mathbf{r}'' - \mathbf{r}')d\mathbf{r}'' \quad (2.3)$$

where v is the bare Coulomb interaction and P is the polarization propagator. The simplest approximation for P is the RPA that corresponds to the Hartree approximation for the one particle Green function $G^0(\mathbf{r}, t; \mathbf{r}', t')$. In this approximation, the polarization propagator P^0 is given by

$$P^0(\mathbf{r}, t; \mathbf{r}', t') = -i\hbar G^0(\mathbf{r}, t; \mathbf{r}', t')G^0(\mathbf{r}', t'; \mathbf{r}, t) \quad (2.4)$$

For the case of a solid with translational symmetry we can Fourier transform the equation for the dielectric function Eq. (2.3) to obtain its expression as a tensor in the reciprocal lattice vectors:

$$\epsilon_{\mathbf{G}, \mathbf{G}'}(\mathbf{q}, \omega) = \delta_{\mathbf{G}, \mathbf{G}'} - v(\mathbf{q} + \mathbf{G})P_{\mathbf{G}, \mathbf{G}'}^0(\mathbf{q}, \omega), \quad (2.5)$$

where $P_{\mathbf{G}, \mathbf{G}'}^0(\mathbf{q}, \omega)$ is the Fourier transform in the lattice of the bare polarizability defined in Eq. (2.4). It is given by

$$P_{\mathbf{G}, \mathbf{G}'}^0(\mathbf{q}, \omega) = \frac{1}{\Omega_c} \sum_{n', n, \mathbf{k}} \frac{f_0(\varepsilon_{n, \mathbf{k} + \mathbf{q}}) - f_0(\varepsilon_{n', \mathbf{k}})}{\varepsilon_{n, \mathbf{k} + \mathbf{q}} - \varepsilon_{n', \mathbf{k}} - \omega} [M_{n', n}^{\mathbf{G}}(\mathbf{k}, \mathbf{q})]^* M_{n', n}^{\mathbf{G}'}(\mathbf{k}, \mathbf{q}), \quad (2.6)$$

with the matrix elements M defined as

$$M_{n', n}^{\mathbf{G}}(\mathbf{k}, \mathbf{q}) = \langle n', \mathbf{k} | e^{-i(\mathbf{q} + \mathbf{G}) \cdot \mathbf{r}} | n, \mathbf{k} + \mathbf{q} \rangle. \quad (2.7)$$

The expression obtained so far is the dielectric tensor that connects the total electrostatic potential in the solid, V , with the potential produced only by the external sources, V^{ext} , through the expression

$$V_{\mathbf{G}}^{ext}(\mathbf{q}, \omega) = \sum_{\mathbf{G}'} \epsilon_{\mathbf{G}, \mathbf{G}'}(\mathbf{q}, \omega) V_{\mathbf{G}'}(\mathbf{q}, \omega). \quad (2.8)$$

If we denote by $\bar{\epsilon}$ the inverse of the dielectric tensor, we can invert the relation above to obtain an expression for the total potential

$$V_{\mathbf{G}}(\mathbf{q}, \omega) = \sum_{\mathbf{G}'} \bar{\epsilon}_{\mathbf{G}, \mathbf{G}'}(\mathbf{q}, \omega) V_{\mathbf{G}'}^{ext}(\mathbf{q}, \omega). \quad (2.9)$$

When considering perturbations produced by light, only long wavelength components are present in the external perturbation potential. Therefore, it is enough to assume that only the $\mathbf{G} = 0$ component is different from zero. In this case the response is

$$V_{\mathbf{G}}(\mathbf{q}, \omega) = \bar{\epsilon}_{\mathbf{G},0}(\mathbf{q}, \omega) V_0^{ext}(\mathbf{q}, \omega) . \quad (2.10)$$

This expression shows that even in the case of an external potential with long wavelength variations in space, the response of the solid will have shorter wavelength components that are commonly called local field effects. The macroscopic dielectric constant ϵ_M , related to the measured optical properties in solids is the ratio between the average of the total potential in one unit cell, i.e. $V_0(\mathbf{q}, \omega)$, and the external field. In this way we identify the macroscopic dielectric constant

$$\epsilon_M(\mathbf{q}, \omega) = \frac{1}{\bar{\epsilon}_{0,0}(\mathbf{q}, \omega)} \quad (2.11)$$

by the $(0, 0)$ element of the *inverse* dielectric tensor.

The expression for the macroscopic dielectric constant given in Eq. (2.11) is rather costly to evaluate. It involves the evaluation of the dielectric tensor with components $(\mathbf{G}, \mathbf{G}')$ up to a certain cutoff and the subsequent inversion to obtain the $(0, 0)$ component of the inverse tensor. It is a common simplification to neglect the local field effects and replace the $(0, 0)$ component of the inverse by the inverse of the $(0, 0)$ component to obtain

$$\epsilon_M^{\{nlf\}}(\mathbf{q}, \omega) = \epsilon_{0,0}(\mathbf{q}, \omega) = 1 - v(\mathbf{q}) P_{0,0}^0(\mathbf{q}, \omega) . \quad (2.12)$$

We are going to neglect local field effects for the rest of the paper in order to give the zero order theory evaluated with the Kohn-Sham eigenvalues and eigenvectors from LAPW, one of the most precise electronic structure methods available. Further improvements of the theory can be introduced by including these local field effects or a better many body description of the electron system. Our results will be the starting point where no basis set effect can be blamed for inaccuracies. Early attempts to include local field corrections by Stephen Adler⁶, and independently but in the same spirit by Nathan Wiser⁷ found that, in a first approximation, these effects can be described by the Lorenz-Lorentz formula with a renormalized polarizability. The effect turned out to be quite small for most Fermi surfaces studied. More recently, it has been found that local field effects are important for high energy excitations where localized states are involved.¹⁰

The Lindhard expression for the dielectric constant of Eq. (2.1) can be obtained from the expression of the macroscopic dielectric constant without local field effects (Eq. (2.12)) by assuming that the electron system is composed by only one band and the matrix elements are equal to one. This is the case for a simple parabolic band of free electrons.

Since we are interested in the optical properties of solids, and the wavevector of light \mathbf{q} is much smaller than any typical wavevector of electrons in the system, we need to evaluate the polarizability P entering in Eq. (2.12) in the limit of $\mathbf{q} \rightarrow 0$. The matrix elements involved in the expression for P given in Eq. (2.6) and defined in Eq. (2.7) can be evaluated for small \mathbf{q} by perturbation theory. We will show the details in Appendix VIB, where the result is given in Eq. (6.17). This expression shows that the limit is different for intraband matrix elements, i.e., those with $n' = n$, and for interband matrix elements. According to this observation it is convenient to split the sum over n' and n into those terms with $n' = n$, corresponding to electronic transitions in the same band, and those with $n' \neq n$ corresponding to interband transitions. In this manner, we can write

$$\epsilon_M^{\{\text{nlf}\}}(\mathbf{q} \rightarrow 0, \omega) = 1 + \epsilon^{\{\text{intra}\}}(\mathbf{q} \rightarrow 0, \omega) + \epsilon^{\{\text{inter}\}}(\mathbf{q} \rightarrow 0, \omega), \quad (2.13)$$

where the intraband part of the dielectric constant is given by

$$\epsilon^{\{\text{intra}\}}(\mathbf{q} \rightarrow 0, \omega) = - \lim_{\mathbf{q} \rightarrow 0} \frac{4\pi e^2}{\Omega_c |\mathbf{q}|^2} \sum_{n, \mathbf{k}} \frac{f_0(\varepsilon_{n, \mathbf{k} + \mathbf{q}}) - f_0(\varepsilon_{n, \mathbf{k}})}{\varepsilon_{n, \mathbf{k} + \mathbf{q}} - \varepsilon_{n, \mathbf{k}} - \omega} |M_{n, n}^0(\mathbf{k}, \mathbf{q})|^2, \quad (2.14)$$

and the interband part by

$$\epsilon^{\{\text{inter}\}}(\mathbf{q} \rightarrow 0, \omega) = - \lim_{\mathbf{q} \rightarrow 0} \frac{4\pi e^2}{\Omega_c |\mathbf{q}|^2} \sum_{n', n \neq n', \mathbf{k}} \frac{f_0(\varepsilon_{n', \mathbf{k} + \mathbf{q}}) - f_0(\varepsilon_{n, \mathbf{k}})}{\varepsilon_{n', \mathbf{k} + \mathbf{q}} - \varepsilon_{n, \mathbf{k}} - \omega} |M_{n, n'}^0(\mathbf{k}, \mathbf{q})|^2. \quad (2.15)$$

While taking the limit of $\mathbf{q} \rightarrow 0$ we can use the expression of the matrix element evaluated in Eq. (6.17) and the expansion of the band energies obtained in Eq. (6.15) to obtain for the intraband part

$$\epsilon^{\{\text{intra}\}}(\mathbf{q} \rightarrow 0, \omega) = - \lim_{\mathbf{q} \rightarrow 0} \frac{4\pi \hbar^2 e^2}{\Omega_c m^2 \omega^2} \sum_{n, \mathbf{k}} \left(- \frac{\partial f}{\partial \varepsilon} \right)_{\varepsilon_{n, \mathbf{k}}} \left(\mathbf{p}_{n, n, \mathbf{k}} \cdot \frac{\mathbf{q}}{|\mathbf{q}|} \right)^2, \quad (2.16)$$

where the derivative of the Fermi function with respect to the energy should be considered as a restriction to sum only over the states at the Fermi level. The momentum matrix element $\mathbf{p}_{n, l, \mathbf{k}}$ is defined in Eq.(6.13) and evaluated for the LAPW basis set in Section IIIB. The interband expression is

$$\epsilon^{\{\text{inter}\}}(\mathbf{q} \rightarrow 0, \omega) = - \lim_{\mathbf{q} \rightarrow 0} \frac{4\pi \hbar^2 e^2}{\Omega_c m^2} \sum_{\mathbf{k}} \sum_{c, v} \frac{(\mathbf{p}_{c, v, \mathbf{k}} \cdot \mathbf{q} / |\mathbf{q}|)^2}{(\varepsilon_{c, \mathbf{k}} - \varepsilon_{v, \mathbf{k}} - \omega) (\varepsilon_{c, \mathbf{k}} - \varepsilon_{v, \mathbf{k}})^2}, \quad (2.17)$$

where, for a given \mathbf{k} , c runs over the empty states and v over the occupied states.

From these expressions, we see that the limit is not well defined and the result depends on the direction of the vector \mathbf{q} even when the limit is taken. This defines the dielectric constant for $\mathbf{q} \rightarrow 0$ as a three dimensional tensor, the dielectric tensor given by

$$\begin{aligned} \epsilon_{i,j}(\omega) = & \delta_{i,j} \\ & - \frac{4\pi\hbar^2 e^2}{\Omega_c m^2 \omega^2} \sum_{n,\mathbf{k}} \left(-\frac{\partial f}{\partial \epsilon} \right)_{\epsilon_{n,\mathbf{k}}} p_{i;n,n,\mathbf{k}} p_{j;n,n,\mathbf{k}} \\ & - \frac{4\pi\hbar^2 e^2}{\Omega_c m^2} \sum_{\mathbf{k}} \sum_{c,v} \frac{p_{i;c,v,\mathbf{k}} p_{j;c,v,\mathbf{k}}}{(\epsilon_{c,\mathbf{k}} - \epsilon_{v,\mathbf{k}} - \omega)(\epsilon_{c,\mathbf{k}} - \epsilon_{v,\mathbf{k}})^2}. \end{aligned} \quad (2.18)$$

It is clear that in the derivation of the RPA formulas presented here the unperturbed electronic states are described by the bare one-particle propagator G^0 . In the Kohn-Sham approximation the many-body problem was reduced to the solution of N one-body problems. These single-particle problems are not representing bare particles but an effective decoupling through the introduction of independent quasiparticles. If the decoupling is done with the Hartree-Fock approximation, the scheme we just presented is conserving in the Kadanoff-Baym⁹ sense. Here, we are going to use the RPA expression for the dielectric constant evaluated with the KS orbitals. This is equivalent to assume that the frequency dependent exchange and correlation kernel of TDDFT is zero, which represents a non conserving approximation to the problem. Nevertheless, in order to gain physical insight into the applicability and limitations of this procedure, we will use the RPA formula utilizing the KS orbitals as our approximation to the dielectric constant. This procedure is also called the independent particle approximation because it neglects the electron-hole interaction during the absorption process. This should be a good approximation for metals due to the more effective screening of the Coulomb interaction compared to semiconductors. Comparison between our results and experimental data is an important step in the validation of this approach. It also allows to compare, when possible, with the results of more elaborated schemes to treat the many body effects as GW, the solution of the Bethe-Salpeter-Equation (BSE), or different frequency dependent kernels in TDDFT.

At the end of this Section, we give the expressions which will be finally computed. Most important is the imaginary part of the interband contribution to the dielectric tensor com-

ponents:

$$\epsilon_{ij}^{\{\text{inter}\}}(\omega) = \frac{\hbar^2 e^2}{\pi m^2 \omega^2} \sum_{n,n'} \int_{\mathbf{k}} p_{i;n',n,\mathbf{k}} p_{j;n,n,\mathbf{k}} (f(\varepsilon_{n,\mathbf{k}}) - f(\varepsilon_{n',\mathbf{k}})) \delta(\varepsilon_{n',\mathbf{k}} - \varepsilon_{n,\mathbf{k}} - \omega) \quad (2.19)$$

The corresponding real parts are obtained by Kramers-Kronig transformation.

As it is evident from Eq. (2.18), the intraband part is singular at $\omega = 0$. At this point the plasma frequency $\omega_{pl;ij}$ is defined by:

$$\omega_{pl;ij}^2 = \frac{\hbar^2 e^2}{\pi m^2} \sum_n \int_{\mathbf{k}} p_{i;n,n,\mathbf{k}} p_{j;n,n,\mathbf{k}} \delta(\varepsilon_{n,\mathbf{k}} - \varepsilon_F) \quad (2.20)$$

In practical calculations, a lifetime broadening Γ is introduced adopting a Drude-like shape for the intraband contribution. $\epsilon_{ij}^{\{\text{intra}\}}(\omega)$ then reads:

$$\text{Im}\epsilon_{ij}^{\{\text{intra}\}}(\omega) = \frac{\Gamma \omega_{pl;ij}^2}{\omega(\omega^2 + \Gamma^2)} \quad (2.21)$$

$$\text{Re}\epsilon_{ij}^{\{\text{intra}\}}(\omega) = 1 - \frac{\omega_{pl;ij}^2}{(\omega^2 + \Gamma^2)} \quad (2.22)$$

Note that the imaginary part is still singular; therefore one usually works with the optical conductivity. The BZ integrations in Eqs. (2.19) and (2.20) are carried out by the linear tetrahedron method.

B. Symmetry

The dielectric tensor is symmetric with up to six independent components according to the symmetry of the crystal. Therefore the general expression for the imaginary part of ϵ is:

$$\begin{pmatrix} \text{Im } \epsilon_{xx} & \text{Im } \epsilon_{xy} & \text{Im } \epsilon_{xz} \\ \text{Im } \epsilon_{xy} & \text{Im } \epsilon_{yy} & \text{Im } \epsilon_{yz} \\ \text{Im } \epsilon_{xz} & \text{Im } \epsilon_{yz} & \text{Im } \epsilon_{zz} \end{pmatrix} \quad (2.23)$$

For orthorhombic or higher symmetry only diagonal components exist. In case of cubic symmetry the optical properties are isotropic, i.e., there is only one independent component $\text{Im } \epsilon_{xx}$, while for uniaxial symmetry (tetragonal, hexagonal) and orthorhombic symmetry there are two and three independent components, respectively. In the monoclinic case non-

diagonal elements occur, i.e for $\gamma \neq 90^\circ$ the tensor takes the form:

$$\begin{pmatrix} \text{Im } \epsilon_{xx} & \text{Im } \epsilon_{xy} & 0 \\ \text{Im } \epsilon_{xy} & \text{Im } \epsilon_{yy} & 0 \\ 0 & 0 & \text{Im } \epsilon_{zz} \end{pmatrix} \quad (2.24)$$

These materials are optically active or birefringent. Only in the triclinic crystal all six components are different.

These symmetry considerations only hold for non-relativistic and scalar-relativistic calculations. In these cases the spin-up and spin-down elements can be evaluated separately, where the corresponding real parts are obtained by the Kramers–Kronig transformation (see below). In case of magento-optics the symmetry is reduced by the presence of a magnetic field as well as by the loss of time-reversal symmetry due to spin-orbit coupling. The latter gives rise to antisymmetric non-diagonal components, e.g. for the magnetic field parallel to z :

$$\begin{pmatrix} 0 & \text{Re } \epsilon_{xy} & 0 \\ -\text{Re } \epsilon_{xy} & 0 & 0 \\ 0 & 0 & 0 \end{pmatrix}. \quad (2.25)$$

The corresponding imaginary parts are again obtained by Kramers–Kronig analysis. In case of monoclinic or lower symmetry the off-diagonal elements can therefore have two independent contributions, one due to a non-orthogonal crystal axis, and the other one due to the magneto-optical effect.

C. Kramers–Kronig relations and optical constants

From the imaginary part of the dielectric tensor component $\text{Im } \epsilon_{ij}$ the corresponding real part is obtained by

$$\text{Re } \epsilon_{ij} = \delta_{ij} + \frac{2}{\pi} \wp \int_0^\infty \frac{\omega' \text{Im } \epsilon_{ij}(\omega')}{\omega'^2 - \omega^2} d\omega'. \quad (2.26)$$

Given the real part, the inverse transformation has to be used.

With the knowledge of the complex dielectric tensor components all other frequency-dependent optical "constants" can be obtained. The most often used ones are the real part of the optical conductivity

$$\text{Re } \sigma_{ij}(\omega) = \frac{\omega}{4\pi} \text{Im } \epsilon_{ij}(\omega), \quad (2.27)$$

the loss function

$$L_{ij}(\omega) = -\text{Im} \left(\frac{1}{\epsilon_{ij}(\omega)} \right), \quad (2.28)$$

and the reflectivity at normal incidence

$$R_{ii}(\omega) = \frac{(n-1)^2 + k^2}{(n+1)^2 + k^2} \quad (2.29)$$

with n and k being the real and imaginary part of the complex refractive index (refractive index and extinction coefficient):

$$n_{ii}(\omega) = \sqrt{\frac{|\epsilon_{ii}(\omega)| + \text{Re} \epsilon_{ii}(\omega)}{2}} \quad (2.30)$$

$$k_{ii}(\omega) = \sqrt{\frac{|\epsilon_{ii}(\omega)| - \text{Re} \epsilon_{ii}(\omega)}{2}} \quad (2.31)$$

The absorption coefficient is given by

$$A_{ii}(\omega) = \frac{2\omega k(\omega)}{c}. \quad (2.32)$$

Note that the latter formulas only hold for the diagonal form of the tensor.

D. Sumrules

There are three sumrules which obtain information about the absorption process:

$$\int_0^{\omega'} \sigma(\omega) \omega d\omega = N_{eff}(\omega') \quad (2.33)$$

$$\int_0^{\omega'} \text{Im} \left(\frac{-1}{\epsilon(\omega)} \right) \omega d\omega = N_{eff}(\omega') \quad (2.34)$$

$$\int_0^{\infty} \text{Im} \left(\frac{-1}{\epsilon(\omega)} \right) \frac{1}{\omega} d\omega = \frac{\pi}{2} \quad (2.35)$$

The first two give an effective number of electrons contributing to the absorption process as a function of energy. Typically, in the low energy region the contribution to the intraband spectrum should sum up to the number of the outermost valence electrons.

III. OPTICAL RESPONSE WITHIN THE LAPW METHOD

A. The LAPW basis set

In bandstructure calculations based on density-functional theory¹ the single-particle electronic states $\Psi_{n\mathbf{k}}(\mathbf{r})$ and energies $\varepsilon_{n\mathbf{k}}$ are described by the solutions of the Kohn-Sham (KS) equation²

$$\left[-\frac{\hbar^2}{2m}\nabla^2 + V_{eff}(\mathbf{r}) \right] \Psi_{n\mathbf{k}}(\mathbf{r}) = \varepsilon_{n\mathbf{k}} \Psi_{n\mathbf{k}}(\mathbf{r}) \quad (3.1)$$

with the effective potential $V_{eff}(\mathbf{r})$ being the sum of the bare Coulomb potential of the atomic nuclei $V_{latt}(\mathbf{r})$, the Hartree potential $V_H(\mathbf{r})$ and the exchange correlation potential $V_{xc}(\mathbf{r})$. In practical calculations, Eq. (3.1) is solved via the Rayleigh-Ritz variational principle. In this procedure the electronic states $\Psi_{n\mathbf{k}}(\mathbf{r})$ (KS-orbitals) are first expanded in terms of a physically appropriate finite set of basis functions $\{\phi_{\mathbf{k}+\mathbf{G}}\}$,

$$\Psi_{n\mathbf{k}}(\mathbf{r}) = \sum_{\mathbf{G}} C_{n\mathbf{k}}(\mathbf{G}) \phi_{\mathbf{k}+\mathbf{G}}(\mathbf{r}) \quad (3.2)$$

with \mathbf{G} and $C_{n\mathbf{k}}(\mathbf{G})$ denoting a reciprocal lattice vector, and the corresponding variational coefficient, respectively. To determine $C_{n\mathbf{k}}(\mathbf{G})$ the ansatz (3.2) is inserted into Eq. (3.1) followed by the minimization of the total crystal energy with respect to the variational coefficients. The eigenvectors and eigenvalues of the resulting matrix equation,

$$\sum_{\mathbf{G}'} (H_{\mathbf{k}+\mathbf{G},\mathbf{k}+\mathbf{G}'} - \varepsilon_{n\mathbf{k}} S_{\mathbf{k}+\mathbf{G},\mathbf{k}+\mathbf{G}'}) C_{n\mathbf{k}}(\mathbf{G}') = 0 \quad \mathbf{k} \in \text{BZ} \quad (3.3)$$

with

$$H_{\mathbf{k}+\mathbf{G},\mathbf{k}+\mathbf{G}'} \equiv \langle \phi_{\mathbf{k}+\mathbf{G}} \left| -\frac{\hbar^2}{2m}\nabla^2 + V_{eff} \right| \phi_{\mathbf{k}+\mathbf{G}'} \rangle_{\Omega_c} \quad (3.4)$$

$$S_{\mathbf{k}+\mathbf{G},\mathbf{k}+\mathbf{G}'} \equiv \langle \phi_{\mathbf{k}+\mathbf{G}} | \phi_{\mathbf{k}+\mathbf{G}'} \rangle_{\Omega_c} \quad (3.5)$$

being Hamilton and overlap matrix, respectively, finally provide the numerical values for $C_{n\mathbf{k}}(\mathbf{G})$ and $\varepsilon_{n\mathbf{k}}$. Ω_c is the volume of the unit cell which in the LAPW method^{11,12} is partitioned into an interstitial region (I) and non-overlapping muffin-tin spheres (MT $_{\alpha}$) centered on the atomic nuclei. The corresponding basis functions are defined as,

$$\phi_{\mathbf{k}+\mathbf{G}}(\mathbf{r}) = \frac{1}{\sqrt{\Omega_c}} e^{i(\mathbf{k}+\mathbf{G})\mathbf{r}}, \quad \mathbf{r} \in \text{I} \quad (3.6)$$

and

$$\phi_{\mathbf{k}+\mathbf{G}}(\mathbf{S}_\alpha + \mathbf{r}) = \sum_{lm} \underbrace{[A_{lm}^\alpha(\mathbf{k} + \mathbf{G})u_l^\alpha(r, E_l) + B_{lm}^\alpha(\mathbf{k} + \mathbf{G})\dot{u}_l^\alpha(r, E_l)]}_{W_{lm}^{\alpha, \mathbf{k}+\mathbf{G}}} Y_{l,m}(\hat{\mathbf{r}}) \quad (3.7)$$

$$= \sum_{lm} W_{lm}^{\alpha, \mathbf{k}+\mathbf{G}}(r, E_l) Y_{l,m}(\hat{\mathbf{r}}) \quad |\mathbf{r}| \leq R_\alpha, \quad (3.8)$$

where \mathbf{S}_α denotes the position vector of the atomic nucleus α . The radius of the corresponding muffin-tin sphere is R_α . The product of the spherical harmonic $Y_{l,m}(\hat{\mathbf{r}})$ and the radial function $u_l^\alpha(r)$ is the solution of the Schrödinger equation for a spherical symmetric potential where the eigenvalue has been replaced by an appropriate energy parameter. The second radial function $\dot{u}_l^\alpha(r)$ is the derivative of the first one with respect to the energy. The coefficients $A_{lm}^\alpha(\mathbf{k} + \mathbf{G})$ and $B_{lm}^\alpha(\mathbf{k} + \mathbf{G})$ are determined for each atom by imposing the requirements that the basis function has to be continuous in value and slope on the MT-surfaces:

$$A_{lm}^\alpha(\mathbf{k} + \mathbf{G}) = \frac{4\pi}{\sqrt{\Omega}} i^l Y_{lm}^* \left(\widehat{\mathbf{k} + \mathbf{G}} \right) R_\alpha^2 e^{i(\mathbf{k}+\mathbf{G})\mathbf{S}_\alpha} a_l(\mathbf{k} + \mathbf{G}) \quad (3.9)$$

$$B_{lm}^\alpha(\mathbf{k} + \mathbf{G}) = \frac{4\pi}{\sqrt{\Omega}} i^l Y_{lm}^* \left(\widehat{\mathbf{k} + \mathbf{G}} \right) R_\alpha^2 e^{i(\mathbf{k}+\mathbf{G})\mathbf{S}_\alpha} b_l(\mathbf{k} + \mathbf{G}) \quad (3.10)$$

with

$$a_l = j_l'(|\mathbf{k} + \mathbf{G}|R_\alpha) \dot{u}_l(R_\alpha) - j_l(|\mathbf{k} + \mathbf{G}|R_\alpha) \dot{u}_l'(R_\alpha) \quad (3.11)$$

$$b_l = j_l(|\mathbf{k} + \mathbf{G}|R_\alpha) u_l(R_\alpha) - j_l'(|\mathbf{k} + \mathbf{G}|R_\alpha) u_l'(R_\alpha) \quad (3.12)$$

For the explicit evaluation of the Hamilton matrix elements (3.4) an appropriate dual representation of the effective potential is needed. Within the atomic spheres the potential is expanded into spherical harmonics and in the interstitial it is represented by a Fourier series.

B. The momentum matrix elements

Due to the dual representation of the LAPW basis functions, the momentum matrix element is a sum of contributions from the atomic spheres as well as from the interstitial region:

$$\langle n'\mathbf{k} | \mathbf{p} | n\mathbf{k} \rangle = \sum_{\alpha} \langle n'\mathbf{k} | \mathbf{p} | n\mathbf{k} \rangle_{\text{MT}_\alpha} + \langle n'\mathbf{k} | \mathbf{p} | n\mathbf{k} \rangle_{\text{I}} \quad (3.13)$$

1. Contributions from the atomic spheres

The usage of spherical harmonics in the LAPW basis set suggest to calculate the expressions $\langle n'\mathbf{k} | \partial x + i\partial y | n\mathbf{k} \rangle$ and $\langle n'\mathbf{k} | \partial x - i\partial y | n\mathbf{k} \rangle$ and to derive the x - and y - component as their linear combinations. Taking into account the ansatz (3.2) for the wavefunctions the following expressions have to be evaluated:

$${}^\alpha \Phi_{\mathbf{k}+\mathbf{G}',\mathbf{k}+\mathbf{G}}^{x+iy} \equiv \langle \phi_{\mathbf{k}+\mathbf{G}'}(\mathbf{S}_\alpha + \mathbf{r}) | \partial x + i\partial y | \phi_{\mathbf{k}+\mathbf{G}}(\mathbf{S}_\alpha + \mathbf{r}) \rangle \quad (3.14)$$

$${}^\alpha \Phi_{\mathbf{k}+\mathbf{G}',\mathbf{k}+\mathbf{G}}^{x-iy} \equiv \langle \phi_{\mathbf{k}+\mathbf{G}'}(\mathbf{S}_\alpha + \mathbf{r}) | \partial x - i\partial y | \phi_{\mathbf{k}+\mathbf{G}}(\mathbf{S}_\alpha + \mathbf{r}) \rangle \quad (3.15)$$

$${}^\alpha \Phi_{\mathbf{k}+\mathbf{G}',\mathbf{k}+\mathbf{G}}^z \equiv \langle \phi_{\mathbf{k}+\mathbf{G}'}(\mathbf{S}_\alpha + \mathbf{r}) | \partial z | \phi_{\mathbf{k}+\mathbf{G}}(\mathbf{S}_\alpha + \mathbf{r}) \rangle \quad (3.16)$$

Expressing $\partial x + i\partial y$, $\partial x - i\partial y$, and ∂z in spherical coordinates

$$\partial x \pm i\partial y = \sin \theta e^{\pm i\phi} \frac{\partial}{\partial r} + \frac{1}{r} e^{\pm i\phi} \left(\cos \theta \frac{\partial}{\partial \theta} \pm \frac{i}{\sin \theta} \frac{\partial}{\partial \phi} \right) \quad (3.17)$$

$$\partial z = \cos \theta \frac{\partial}{\partial r} - \frac{1}{r} \sin \theta \frac{\partial}{\partial \theta} \quad (3.18)$$

we can elaborate the matrix elements (3.14–3.16). We explicitly demonstrate the procedure for the first component:

$${}^\alpha \Phi_{\mathbf{k}+\mathbf{G}',\mathbf{k}+\mathbf{G}}^{x+iy} = \langle \phi_{\mathbf{k}+\mathbf{G}'}(\mathbf{S}_\alpha + \mathbf{r}) \left| \sin \theta e^{i\phi} \frac{\partial}{\partial r} + \frac{1}{r} e^{i\phi} \left(\cos \theta \frac{\partial}{\partial \theta} + \frac{i}{\sin \theta} \frac{\partial}{\partial \phi} \right) \right| \phi_{\mathbf{k}+\mathbf{G}}(\mathbf{S}_\alpha + \mathbf{r}) \rangle \quad (3.19)$$

Here the first term of the operator acts on the radial coordinate only, whereas the second term acts on the angular coordinates only. Applying this operator to the LAPW basis functions (3.8) one obtains:

$$\begin{aligned} (\partial x + i\partial y) \phi_{\mathbf{k}+\mathbf{G}}(\mathbf{S}_\alpha + \mathbf{r}) &= \sum_{lm} \frac{\partial}{\partial r} W_{lm}^{\alpha,\mathbf{k}+\mathbf{G}}(r) \sin \theta e^{i\phi} Y_{l,m}(\hat{\mathbf{r}}) + \\ &\frac{1}{r} \sum_{lm} W_{lm}^{\alpha,\mathbf{k}+\mathbf{G}}(r) e^{i\phi} \left(\cos \theta \frac{\partial}{\partial \theta} + \frac{i}{\sin \theta} \frac{\partial}{\partial \phi} \right) Y_{l,m}(\hat{\mathbf{r}}) \end{aligned} \quad (3.20)$$

Exploiting the relations between the spherical harmonics as summarized in the Appendix, and omitting the arguments of the spherical harmonics for simplicity, Eq. (3.20) becomes

$$\begin{aligned} (\partial x + i\partial y) \phi_{\mathbf{k}+\mathbf{G}}(\mathbf{S}_\alpha + \mathbf{r}) &= \sum_{lm} \left[\frac{\partial}{\partial r} W_{lm}^{\alpha,\mathbf{k}+\mathbf{G}}(r) - \frac{l}{r} W_{lm}(r) \right] F_{l,m}^{(1)} Y_{l+1,m+1} + \\ &\left[\frac{\partial}{\partial r} W_{lm}^{\alpha,\mathbf{k}+\mathbf{G}}(r) + \frac{l+1}{r} W_{lm}(r) \right] F_{l,m}^{(2)} Y_{l-1,m+1}. \end{aligned} \quad (3.21)$$

The $x + iy$ component will then be

$$\begin{aligned}
\alpha \Phi_{\mathbf{k}+\mathbf{G}',\mathbf{k}+\mathbf{G}}^{x+iy} &= \int_{\text{MT}_\alpha} \phi_{\mathbf{k}+\mathbf{G}'}(\mathbf{S}_\alpha + \mathbf{r}) [\partial x + i\partial y] \phi_{\mathbf{k}+\mathbf{G}}(\mathbf{S}_\alpha + \mathbf{r}) d\mathbf{r} = \\
&\int_0^{R_\alpha} r^2 dr \oint d\Omega \sum_{l'm'} \sum_{lm} W_{l'm'}^{*\alpha,\mathbf{k}+\mathbf{G}'} Y_{l',m'}^* \times \\
&\left(\left[\frac{\partial}{\partial r} W_{lm}^{\alpha,\mathbf{k}+\mathbf{G}}(r) - \frac{l}{r} W_{lm}(r) \right] F_{l,m}^{(1)} Y_{l+1,m+1} + \left[\frac{\partial}{\partial r} W_{lm}^{\alpha,\mathbf{k}+\mathbf{G}}(r) + \frac{l+1}{r} W_{lm}(r) \right] F_{l,m}^{(2)} Y_{l-1,m+1} \right) = \\
&\sum_{l'm'} \sum_{lm} \underbrace{\int_0^{R_\alpha} r^2 dr W_{l'm'}^{*\alpha,\mathbf{k}+\mathbf{G}'} \left[\frac{\partial}{\partial r} W_{lm}^{\alpha,\mathbf{k}+\mathbf{G}}(r) - \frac{l}{r} W_{lm}(r) \right] F_{l,m}^{(1)}}_{R_{l,m}^{l',m'}(r)} \underbrace{\oint d\Omega Y_{l',m'}^* Y_{l+1,m+1}}_{\delta_{l',l+1} \delta_{m',m+1}} + \\
&\sum_{l'm'} \sum_{lm} \underbrace{\int_0^{R_\alpha} r^2 dr W_{l'm'}^{*\alpha,\mathbf{k}+\mathbf{G}'} \left[\frac{\partial}{\partial r} W_{lm}^{\alpha,\mathbf{k}+\mathbf{G}}(r) + \frac{l+1}{r} W_{lm}(r) \right] F_{l,m}^{(2)}}_{T_{l,m}^{l',m'}(r)} \underbrace{\oint d\Omega Y_{l',m'}^* Y_{l-1,m+1}}_{\delta_{l',l-1} \delta_{m',m+1}}. \tag{3.22}
\end{aligned}$$

Writing explicitly the sums over $l, m, l',$ and $m',$ taking into account an upper limit l_{max} for l we obtain:

$$\begin{aligned}
\alpha \Phi_{\mathbf{k}+\mathbf{G}',\mathbf{k}+\mathbf{G}}^{x+iy} &= \sum_{l'=0}^{lmax} \sum_{m'=-l'}^{l'} \sum_{l=0}^{lmax} \sum_{m=-l}^l R_{l,m}^{l',m'}(r) \delta_{l',l+1} \delta_{m',m+1} + \\
&\sum_{l'=0}^{lmax} \sum_{m'=-l'}^{l'} \sum_{l=0}^{lmax} \sum_{m=-l}^l T_{l,m}^{l',m'}(r) \delta_{l',l-1} \delta_{m',m+1} = \\
&\sum_{l=0}^{lmax-1} \sum_{m=-l}^l \left(R_{l,m}^{l+1,m+1}(r) + T_{l+1,m-1}^{l,m}(r) \right) \tag{3.23}
\end{aligned}$$

Evaluating $R_{l,m}^{l+1,m+1}(r)$ and $T_{l+1,m-1}^{l,m}(r)$ using Eqs. (3.22) and (3.8) we finally obtain:

$$\begin{aligned}
{}^\alpha\Phi_{\mathbf{k}+\mathbf{G}',\mathbf{k}+\mathbf{G}}^{x+iy} = & \sum_{l=0}^{lmax-1} \sum_{m=-l}^l \left\{ F_{lm}^{(1)} \right. \\
& \left\{ A_{l+1,m+1}^{*\alpha}(\mathbf{k} + \mathbf{G}') A_{l,m}^\alpha(\mathbf{k} + \mathbf{G}) \left(\int_0^{R_\alpha} u_{l+1}(r) u_l'(r) r^2 dr - l \int_0^{R_\alpha} u_{l+1}(r) u_l(r) r dr \right) + \right. \\
& A_{l+1,m+1}^{*\alpha}(\mathbf{k} + \mathbf{G}') B_{l,m}^\alpha(\mathbf{k} + \mathbf{G}) \left(\int_0^{R_\alpha} u_{l+1}(r) \dot{u}_l'(r) r^2 dr - l \int_0^{R_\alpha} u_{l+1}(r) \dot{u}_l(r) r dr \right) + \\
& B_{l+1,m+1}^{*\alpha}(\mathbf{k} + \mathbf{G}') A_{l,m}^\alpha(\mathbf{k} + \mathbf{G}) \left(\int_0^{R_\alpha} \dot{u}_{l+1}(r) u_l'(r) r^2 dr - l \int_0^{R_\alpha} \dot{u}_{l+1}(r) u_l(r) r dr \right) + \\
& \left. B_{l+1,m+1}^{*\alpha}(\mathbf{k} + \mathbf{G}') B_{l,m}^\alpha(\mathbf{k} + \mathbf{G}) \left(\int_0^{R_\alpha} \dot{u}_{l+1}(r) \dot{u}_l'(r) r^2 dr - l \int_0^{R_\alpha} \dot{u}_{l+1}(r) \dot{u}_l(r) r dr \right) \right\} \\
& + F_{l+1,m-1}^{(2)} \\
& \left\{ A_{l,m}^{*\alpha}(\mathbf{k} + \mathbf{G}') A_{l+1,m-1}^\alpha(\mathbf{k} + \mathbf{G}) \left(\int_0^{R_\alpha} u_l(r) u_{l+1}'(r) r^2 dr + (l+2) \int_0^{R_\alpha} u_l(r) u_{l+1}(r) r dr \right) + \right. \\
& A_{l,m}^{*\alpha}(\mathbf{k} + \mathbf{G}') B_{l+1,m-1}^\alpha(\mathbf{k} + \mathbf{G}) \left(\int_0^{R_\alpha} u_l(r) \dot{u}_{l+1}'(r) r^2 dr + (l+2) \int_0^{R_\alpha} u_l(r) \dot{u}_{l+1}(r) r dr \right) + \\
& B_{l,m}^{*\alpha}(\mathbf{k} + \mathbf{G}') A_{l+1,m-1}^\alpha(\mathbf{k} + \mathbf{G}) \left(\int_0^{R_\alpha} \dot{u}_l(r) u_{l+1}'(r) r^2 dr + (l+2) \int_0^{R_\alpha} \dot{u}_l(r) u_{l+1}(r) r dr \right) + \\
& \left. B_{l,m}^{*\alpha}(\mathbf{k} + \mathbf{G}') B_{l+1,m-1}^\alpha(\mathbf{k} + \mathbf{G}) \left(\int_0^{R_\alpha} \dot{u}_l(r) \dot{u}_{l+1}'(r) r^2 dr + (l+2) \int_0^{R_\alpha} \dot{u}_l(r) \dot{u}_{l+1}(r) r dr \right) \right\} \Big\} \\
\end{aligned} \tag{3.24}$$

with $u'_l(r)$ denoting $\partial u_l(r)/\partial r$. Analogously we derive the other two components:

$$\begin{aligned}
{}^\alpha \Phi_{\mathbf{k}+\mathbf{G}',\mathbf{k}+\mathbf{G}}^{x-iy} &= \sum_{l=0}^{lmax-1} \sum_{m=-l}^l \left\{ F_{lm}^{(3)} \right. \\
&\left\{ A_{l-1,m+1}^{*\alpha}(\mathbf{k}+\mathbf{G}') A_{l,m}^\alpha(\mathbf{k}+\mathbf{G}) \left(\int_0^{R_\alpha} u_{l+1}(r) u'_l(r) r^2 dr - l \int_0^{R_\alpha} u_{l+1}(r) u_l(r) r dr \right) + \right. \\
&A_{l-1,m+1}^{*\alpha}(\mathbf{k}+\mathbf{G}') B_{l,m}^\alpha(\mathbf{k}+\mathbf{G}) \left(\int_0^{R_\alpha} u_{l+1}(r) \dot{u}'_l(r) r^2 dr - l \int_0^{R_\alpha} u_{l+1}(r) \dot{u}_l(r) r dr \right) + \\
&B_{l-1,m+1}^{*\alpha}(\mathbf{k}+\mathbf{G}') A_{l,m}^\alpha(\mathbf{k}+\mathbf{G}) \left(\int_0^{R_\alpha} \dot{u}_{l+1}(r) u'_l(r) r^2 dr - l \int_0^{R_\alpha} \dot{u}_{l+1}(r) u_l(r) r dr \right) + \\
&B_{l-1,m+1}^{*\alpha}(\mathbf{k}+\mathbf{G}') B_{l,m}^\alpha(\mathbf{k}+\mathbf{G}) \left. \left(\int_0^{R_\alpha} \dot{u}_{l+1}(r) \dot{u}'_l(r) r^2 dr - l \int_0^{R_\alpha} \dot{u}_{l+1}(r) \dot{u}_l(r) r dr \right) \right\} \\
&+ F_{l+1,m-1}^{(4)} \\
&\left\{ A_{l,m}^{*\alpha}(\mathbf{k}+\mathbf{G}') A_{l+1,m+1}^\alpha(\mathbf{k}+\mathbf{G}) \left(\int_0^{R_\alpha} u_l(r) u'_{l+1}(r) r^2 dr + (l+2) \int_0^{R_\alpha} u_l(r) u_{l+1}(r) r dr \right) + \right. \\
&A_{l,m}^{*\alpha}(\mathbf{k}+\mathbf{G}') B_{l+1,m+1}^\alpha(\mathbf{k}+\mathbf{G}) \left(\int_0^{R_\alpha} u_l(r) \dot{u}'_{l+1}(r) r^2 dr + (l+2) \int_0^{R_\alpha} u_l(r) \dot{u}_{l+1}(r) r dr \right) + \\
&B_{l,m}^{*\alpha}(\mathbf{k}+\mathbf{G}') A_{l+1,m+1}^\alpha(\mathbf{k}+\mathbf{G}) \left(\int_0^{R_\alpha} \dot{u}_l(r) u'_{l+1}(r) r^2 dr + (l+2) \int_0^{R_\alpha} \dot{u}_l(r) u_{l+1}(r) r dr \right) + \\
&B_{l,m}^{*\alpha}(\mathbf{k}+\mathbf{G}') B_{l+1,m+1}^\alpha(\mathbf{k}+\mathbf{G}) \left. \left(\int_0^{R_\alpha} \dot{u}_l(r) \dot{u}'_{l+1}(r) r^2 dr + (l+2) \int_0^{R_\alpha} \dot{u}_l(r) \dot{u}_{l+1}(r) r dr \right) \right\} \left. \right\} \quad (3.25)
\end{aligned}$$

$$\begin{aligned}
{}^\alpha \Phi_{\mathbf{k}+\mathbf{G}',\mathbf{k}+\mathbf{G}}^z &= \sum_{l=0}^{lmax-1} \sum_{m=-l}^l \left\{ F_{lm}^{(5)} \right. \\
&\left\{ A_{l+1,m+1}^{*\alpha}(\mathbf{k}+\mathbf{G}') A_{l,m}^\alpha(\mathbf{k}+\mathbf{G}) \left(\int_0^{R_\alpha} u_{l+1}(r) u'_l(r) r^2 dr - l \int_0^{R_\alpha} u_{l+1}(r) u_l(r) r dr \right) + \right. \\
&A_{l+1,m+1}^{*\alpha}(\mathbf{k}+\mathbf{G}') B_{l,m}^\alpha(\mathbf{k}+\mathbf{G}) \left(\int_0^{R_\alpha} u_{l+1}(r) \dot{u}'_l(r) r^2 dr - l \int_0^{R_\alpha} u_{l+1}(r) \dot{u}_l(r) r dr \right) + \\
&B_{l+1,m+1}^{*\alpha}(\mathbf{k}+\mathbf{G}') A_{l,m}^\alpha(\mathbf{k}+\mathbf{G}) \left(\int_0^{R_\alpha} \dot{u}_{l+1}(r) u'_l(r) r^2 dr - l \int_0^{R_\alpha} \dot{u}_{l+1}(r) u_l(r) r dr \right) + \\
&B_{l+1,m+1}^{*\alpha}(\mathbf{k}+\mathbf{G}') B_{l,m}^\alpha(\mathbf{k}+\mathbf{G}) \left. \left(\int_0^{R_\alpha} \dot{u}_{l+1}(r) \dot{u}'_l(r) r^2 dr - l \int_0^{R_\alpha} \dot{u}_{l+1}(r) \dot{u}_l(r) r dr \right) \right\} \\
&+ F_{l+1,m}^{(6)} \\
&\left\{ A_{l,m}^{*\alpha}(\mathbf{k}+\mathbf{G}') A_{l+1,m+1}^\alpha(\mathbf{k}+\mathbf{G}) \left(\int_0^{R_\alpha} u_l(r) u'_{l+1}(r) r^2 dr + (l+2) \int_0^{R_\alpha} u_l(r) u_{l+1}(r) r dr \right) + \right. \\
&A_{l,m}^{*\alpha}(\mathbf{k}+\mathbf{G}') B_{l+1,m+1}^\alpha(\mathbf{k}+\mathbf{G}) \left(\int_0^{R_\alpha} u_l(r) \dot{u}'_{l+1}(r) r^2 dr + (l+2) \int_0^{R_\alpha} u_l(r) \dot{u}_{l+1}(r) r dr \right) + \\
&B_{l,m}^{*\alpha}(\mathbf{k}+\mathbf{G}') A_{l+1,m+1}^\alpha(\mathbf{k}+\mathbf{G}) \left(\int_0^{R_\alpha} \dot{u}_l(r) u'_{l+1}(r) r^2 dr + (l+2) \int_0^{R_\alpha} \dot{u}_l(r) u_{l+1}(r) r dr \right) + \\
&B_{l,m}^{*\alpha}(\mathbf{k}+\mathbf{G}') B_{l+1,m+1}^\alpha(\mathbf{k}+\mathbf{G}) \left. \left(\int_0^{R_\alpha} \dot{u}_l(r) \dot{u}'_{l+1}(r) r^2 dr + (l+2) \int_0^{R_\alpha} \dot{u}_l(r) \dot{u}_{l+1}(r) r dr \right) \right\} \left. \right\} \quad (3.26)
\end{aligned}$$

To obtain the atomic-sphere contributions to the momentum matrix elements, Eqs. (3.14-3.16) have to be multiplied with the variational coefficients and summed up over all basis functions:

$$\begin{aligned}
\langle n'\mathbf{k} | \nabla_x | n\mathbf{k} \rangle_{\text{MT}\alpha} &= \frac{1}{2} \sum_{\mathbf{G}', \mathbf{G}} C_{n'\mathbf{k}}^*(\mathbf{G}') \left({}^\alpha \Phi_{\mathbf{k}+\mathbf{G}', \mathbf{k}+\mathbf{G}}^{x+iy} + {}^\alpha \Phi_{\mathbf{k}+\mathbf{G}', \mathbf{k}+\mathbf{G}}^{x-iy} \right) C_{n\mathbf{k}}(\mathbf{G}) \\
\langle n'\mathbf{k} | \nabla_y | n\mathbf{k} \rangle_{\text{MT}\alpha} &= \frac{1}{2i} \sum_{\mathbf{G}', \mathbf{G}} C_{n'\mathbf{k}}^*(\mathbf{G}') \left({}^\alpha \Phi_{\mathbf{k}+\mathbf{G}', \mathbf{k}+\mathbf{G}}^{x+iy} - {}^\alpha \Phi_{\mathbf{k}+\mathbf{G}', \mathbf{k}+\mathbf{G}}^{x-iy} \right) C_{n\mathbf{k}}(\mathbf{G}) \\
\langle n'\mathbf{k} | \nabla_z | n\mathbf{k} \rangle_{\text{MT}\alpha} &= \sum_{\mathbf{G}', \mathbf{G}} C_{n'\mathbf{k}}^*(\mathbf{G}') {}^\alpha \Phi_{\mathbf{k}+\mathbf{G}', \mathbf{k}+\mathbf{G}}^z C_{n\mathbf{k}}(\mathbf{G})
\end{aligned} \tag{3.27}$$

2. Contributions from the interstitial region

With the planewave basis (3.6) the interstitial contribution to the matrix elements (3.13) can be easily worked out:

$$\langle n'\mathbf{k} | \nabla | n\mathbf{k} \rangle_{\text{I}} = \frac{1}{\Omega_c} \sum_{\mathbf{G}', \mathbf{G}} C_{n'\mathbf{k}}^*(\mathbf{G}') C_{n\mathbf{k}}(\mathbf{G}) \int_{\text{I}} e^{i(\mathbf{G}' - \mathbf{G})\mathbf{r}} d\mathbf{r} \tag{3.28}$$

The integration in Eq. (3.28) over the interstitial region is carried out by integrating over the whole unit cell and subtracting the integral over the atomic spheres (see Appendix).

This procedure finally leads to

$$\begin{aligned}
\langle n'\mathbf{k} | \nabla | n\mathbf{k} \rangle_{\text{I}} &= \frac{i}{\Omega_c} \sum_{\mathbf{G}} (\mathbf{k} + \mathbf{G}) C_{n\mathbf{k}}(\mathbf{G}) \left[C_{n'\mathbf{k}}^*(\mathbf{G}) \left(\Omega_c - \sum_{\alpha} V_{\alpha} \right) - \sum_{\alpha} 3V_{\alpha} \right. \\
&\quad \left. \sum_{\mathbf{G}' \neq \mathbf{G}} C_{n'\mathbf{k}}^*(\mathbf{G}') \frac{\sin(|\mathbf{G}' - \mathbf{G}| R_{\alpha}) - (|\mathbf{G}' - \mathbf{G}| R_{\alpha}) \cos(|\mathbf{G}' - \mathbf{G}| R_{\alpha})}{(|\mathbf{G}' - \mathbf{G}| R_{\alpha})^3} e^{i(\mathbf{G} - \mathbf{G}')\mathbf{s}_{\alpha}} \right], \tag{3.29}
\end{aligned}$$

where V_{α} is the volume of the atomic sphere α .

IV. RESULTS

A. Aluminum

As the first example fcc aluminum has been chosen. It has been intensively studied in literature,^{16,17,18,19,20} where the most puzzling experimental problem at that time was the distinction between interband and intraband contributions to the absorption process. Here, it serves as a test case mainly in terms of convergence with respect to the most important

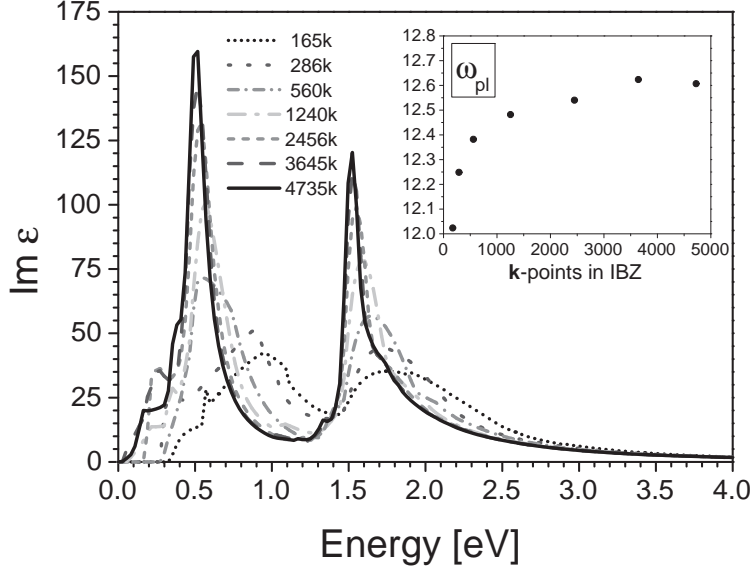


FIG. 1: Imaginary part of the frequency dependent dielectric function of Al for a series of \mathbf{k} point meshes. In the inset the dependence of the plasma frequency (in eV) on the \mathbf{k} point sampling is depicted.

convergence parameters. While the results did not turn out to be sensitive to the number of LAPW's, there is a crucial dependence on the BZ sampling as already found by Lee and Chang.²⁰ Fig. 1 shows the interband contribution to the imaginary part of the dielectric function (Eq. 2.19) for a series of \mathbf{k} point meshes. The peaks do not only get sharper with increasing number of \mathbf{k} points, but they also exhibit a pronounced energy shift. Only with the most dense mesh quantitative agreement with experimental data is achieved.²¹ The inset of Fig. 1 exhibits the plasma frequency (Eq. 2.20) as a function of the number of \mathbf{k} points in the irreducible part of the Brillouin zone (IBZ). Also in this case highest accuracy is needed to reach the converged value of $\omega_{pl} = 12.6 \text{ eV}$. This sensitivity can be understood by the high symmetry of the crystal structure and the simplicity of the material. Since the main contributions stem from certain regions of the BZ,¹⁸ a refinement of the mesh there can dramatically change this contribution and – due to the high weight in the BZ – the total spectrum. In contrast, in more complex materials the optical absorption usually represents a sum of many different contributions from several regions in the BZ and many

band combinations. Therefore a change of one or some of these contributions cannot affect the total spectrum that much. Fig. 2 illustrates the separation of interband and intraband

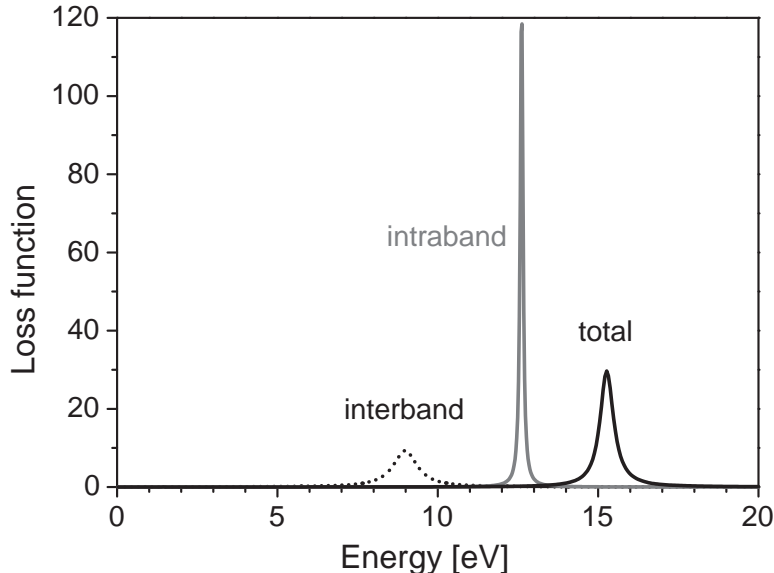


FIG. 2: Loss function for Al (full line) calculated with 4735 \mathbf{k} points in the IBZ. The dashed (dotted) line shows the loss function of the pure intraband (interband) contribution.

contributions to the optical spectra. For this purpose the total loss function is plotted (full line), but also the corresponding functions if there was interband (dotted line) or intraband (dashed line) contributions only. Judging from the shape of the curves all of them could be interpreted as free electron behavior but with very different plasma frequencies. Therefore the plasma frequency was for a long time thought to be 15.2 eV which is the peak position of the total spectrum. For a more detailed discussion of the problem see Ref. 19. Finally the sumrules provide another test for the quality of the calculations. To this extent, all three sumrules as given in Eqs. (2.33 – 2.35) have been tested. In Fig. 3 the results of the corresponding integrations are depicted as a function of energy, i.e. the upper integration limit. The theoretical results for sumrules 2.33 and 2.34 excellently reproduce the region where experimental data are available, while the third curve approaches $\pi/2$ within 0.1 %. Having a closer look to sumrule (1), the kink in the low energy range indicates the setting in of the interband contributions.

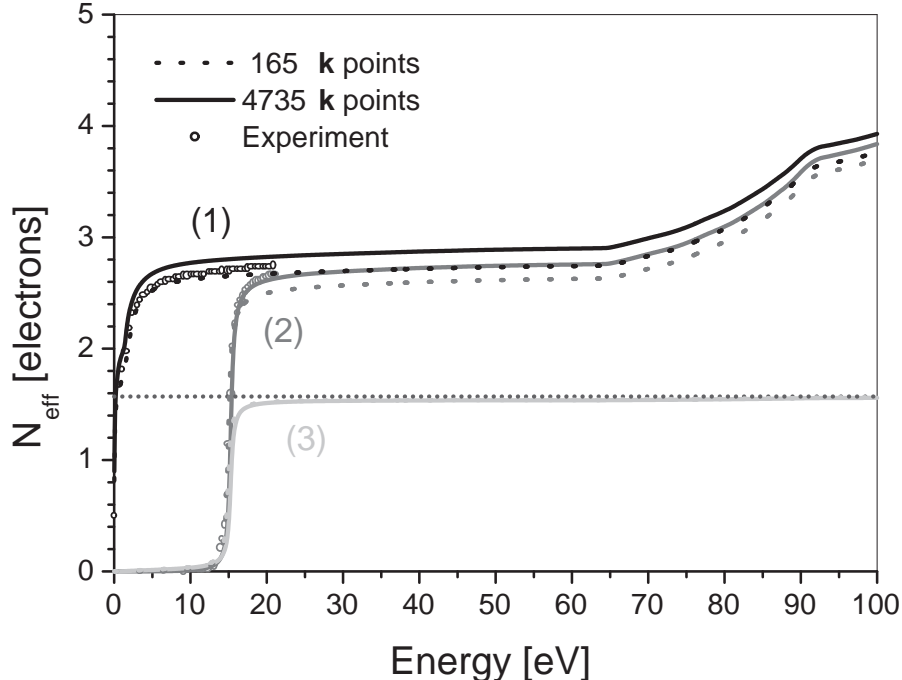


FIG. 3: Sumrule check for the optical spectra of Al by carrying out the integrations given in Eqs. 2.33 (1), 2.34 (2), and 2.35 (3) as a function of the upper integration limit (energy $\hbar\omega$ in eV). The calculated values are given for two different numbers of \mathbf{k} points in the BZ, i.e. 165 (dashed lines) and 4735 (full lines). The corresponding experimental data (open circles) are taken from Ref. 16. The dotted line indicates $\pi/2$ for comparison with the third sumrule (3).

B. Gold

The electronic bands have been studied very intensively in the literature,^{24,25,26,27} and much attention has been paid to relativistic effects on the band structure and henceforth the optical properties.²⁴ But the optical spectra have not been investigated in detail from the first-principles side. Therefore they shall be studied in more detail here.

A lattice parameter of 7.66 a.u. has been taken which is the optimized value with respect to a scalar-relativistic LDA calculation. The self-consistency cycles have been performed with 65 \mathbf{k} points in the IBZ. The BZ integrations for obtaining the density of states (DOS), joint DOS, and the optical properties used in the figures were carried out with 1240 points in the IBZ. (For convergence tests see below.) In order to investigate relativistic effects we have performed *non-relativistic*, *scalar-relativistic*, and *relativistic* calculations, where in the latter spin-orbit coupling has been treated by a second variational scheme. In all cases the

core states are calculated fully relativistically by solving the Dirac equation. We treat the semi-core states $5s$, $5p$ and $4f$ in the valence region by local orbitals. Therefore these low lying states cannot be expected to be very well described in the non-relativistic case. Our procedure, however, has the advantage that the optical properties can be handled by the formalism described above up to high excitation energies which is needed for the Kramers–Kronig analysis as well as for the test of the sumrules. At the same time the influence of relativistic effects can be studied in detail.

Also in the case of gold, we have paid attention to the convergence of the optical spectra with respect to the \mathbf{k} point sampling. It turned out that the density of the \mathbf{k} point mesh is much less important than in aluminum. Already rather coarse meshes give all results with high accuracy. For example, the plasma frequency of the relativistic calculation changes by 0.1 eV only, i.e. from 8.966 to 8.867, when increasing the number of \mathbf{k} points in the IBZ from 165 to 11480. In fact, already with 47 \mathbf{k} points a value of 8.866 eV is obtained. For the interband contributions, the spectra above 2 eV can hardly be distinguished when plotted for different BZ samplings. Only the first interband peak (below 2 eV) in the real part of the dielectric function is somewhat broader with more spectral weight at lower energies when the number of irreducible \mathbf{k} points is reduced below 1240. In Fig. 4 the imaginary part of the dielectric function arising from interband transitions is shown for the three cases mentioned above. While there is hardly any difference between the scalar-relativistic calculation and the treatment including spin-orbit coupling the biggest change is observed when taking into account the scalar-relativistic effects which are due to the Darwin shift and the mass–velocity term.

In order to analyze the origin of these effects the corresponding band structures are shown in Fig. 5. One striking scalar-relativistic effect is the broadening and upward shift of the filled $5d$ bands, which is much bigger than the splitting of some states due to spin-orbit coupling. Also the $5s$ states lying at -9 eV at the Γ point in the non-relativistic case exhibit an increased band width by more than a factor of two. Relativistic effects of the $6s$ and $5p$ states in the conduction band are highlighted in the figure by indicating the predominant band character along the high symmetry lines X–W and W–K. The $5f$ states dominate the band structure above 12 eV in the non-relativistic case, and these bands are pushed up by roughly 1.5 eV. All these effects can be seen more clearly in the total and site-projected densities of states depicted in Fig. 6.

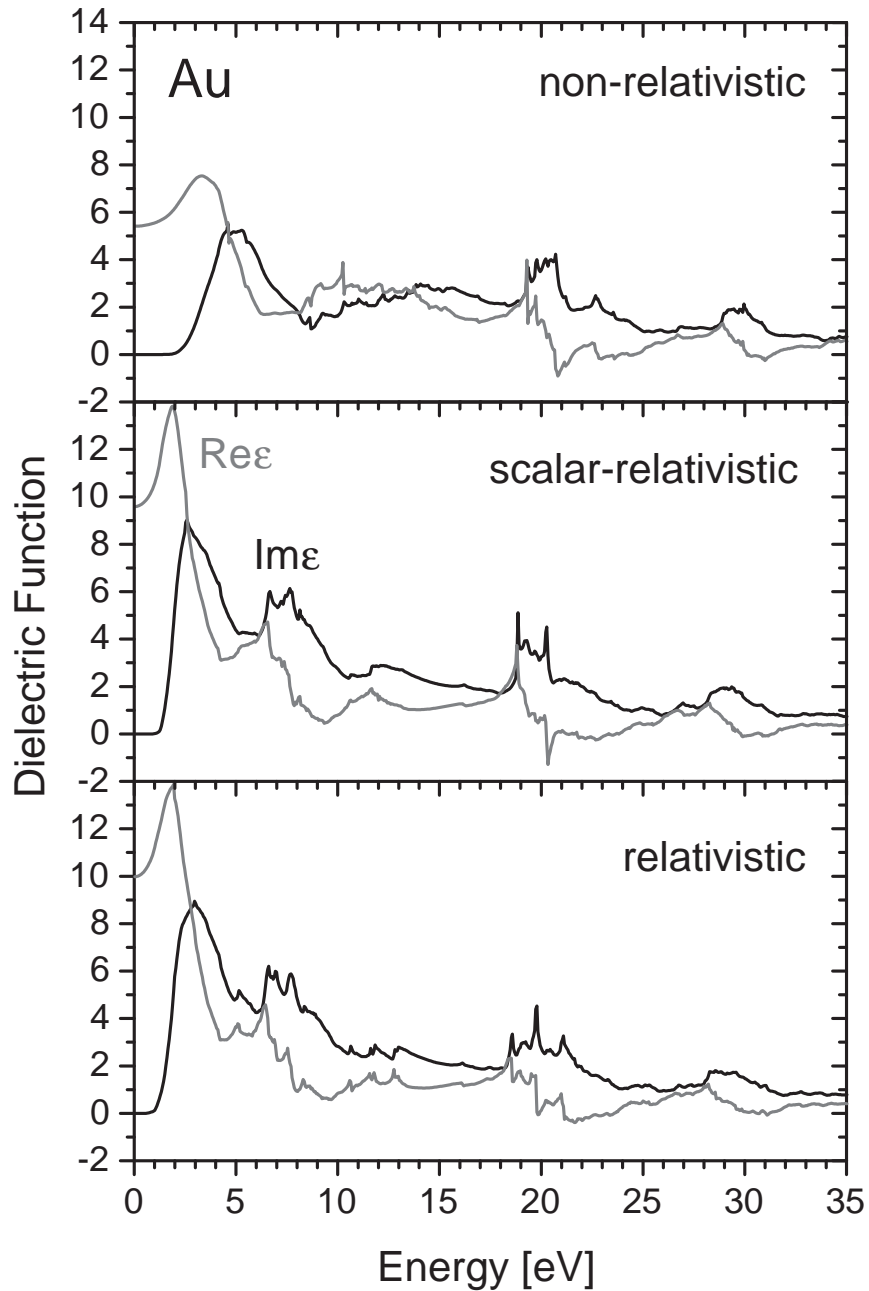


FIG. 4: Interband contribution to the dielectric function of gold: real (grey lines) and imaginary part (black lines) of $\text{Im } \epsilon$ from non-relativistic (top), scalar-relativistic (middle) and relativistic calculations (bottom).

The first half of the spectrum is dominated by transitions between d and p like states which generally are shifted to lower energies due to the upward shift of the d band when relativistic terms are included in the calculations. In particular, the non-relativistic $\text{Im } \epsilon$

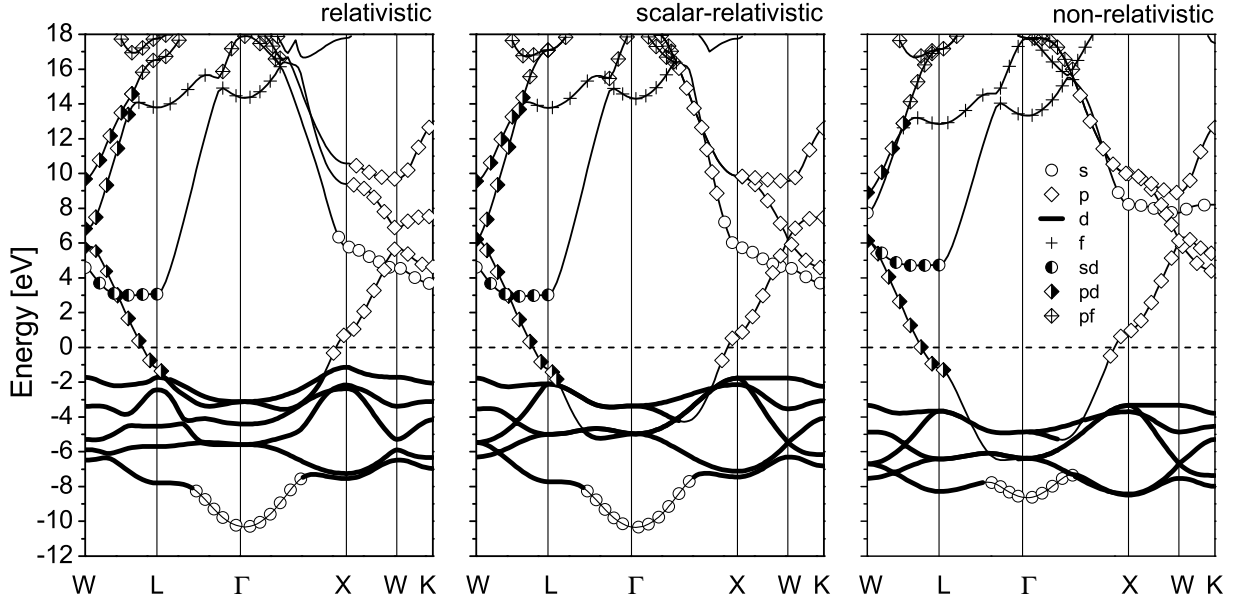


FIG. 5: Relativistic effects in the band structure of gold: non-relativistic (right), scalar-relativistic (middle) and relativistic calculations (left) have been performed. The main l -like band character is highlighted by symbols as indicated in the legend. The thin lines without symbols represent states with more than two different significant contributions.

centered around 5 eV is created by $5d$ to $6p$ transitions with the partially filled band of mainly p character providing the final states. This peak is shifted down by 2 eV in the scalar-relativistic case due to the nearly rigid upward shift of the $5d$ bands. The increase of the spectral weight can be traced back to the $1/\omega^2$ behavior of $\text{Im } \epsilon$. The double peak structure around 6-8 eV visible in the relativistic cases come from transitions from the three highest lying valence levels to the first two unoccupied bands. They also exhibit mainly d to p character, but due to some p admixture in the high lying valence states and a considerable amount of d character in the final states also finite p to d contributions are present. Also the d to f transitions around 20 eV are shifted to lower energies because the f states move up only half as much as the d states. Including spin orbit coupling only very minor changes are obtained. In particular, the d to f transitions are broadened reflecting a splitting of the d bands as can be seen in the band structure and the symmetry projected DOS. The

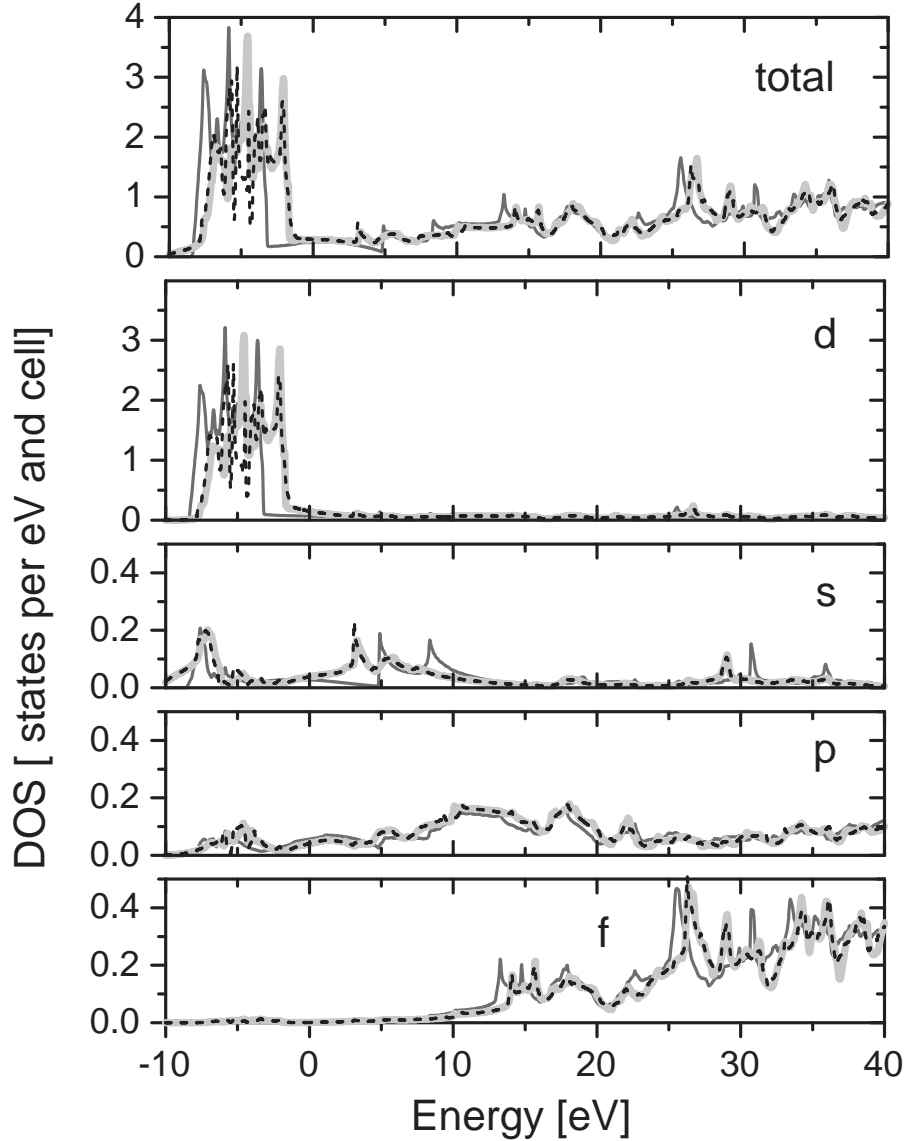


FIG. 6: Total and site-dependent densities of states of Au from a non-relativistic (dark grey), a scalar-relativistic (light grey) and a relativistic calculation (black). spin-orbit coupling

transitions in this case exhibit an asymmetry with respect to the Fermi level. In all cases the initial states are mainly the d bands between -10 and -1 eV, while the final states range from the Fermi level up to very high energies. As already pointed out by Christensen²⁴ the matrix element effect is relatively small. The imaginary part of the dielectric function is already very well estimated by the joint density of states as can be seen in Fig. 7. Since the dielectric function suppresses higher energy transitions due to its $1/\omega^2$ behavior (Eq. 2.5) we have divided the joint DOS by the energy squared. Only a few features there are

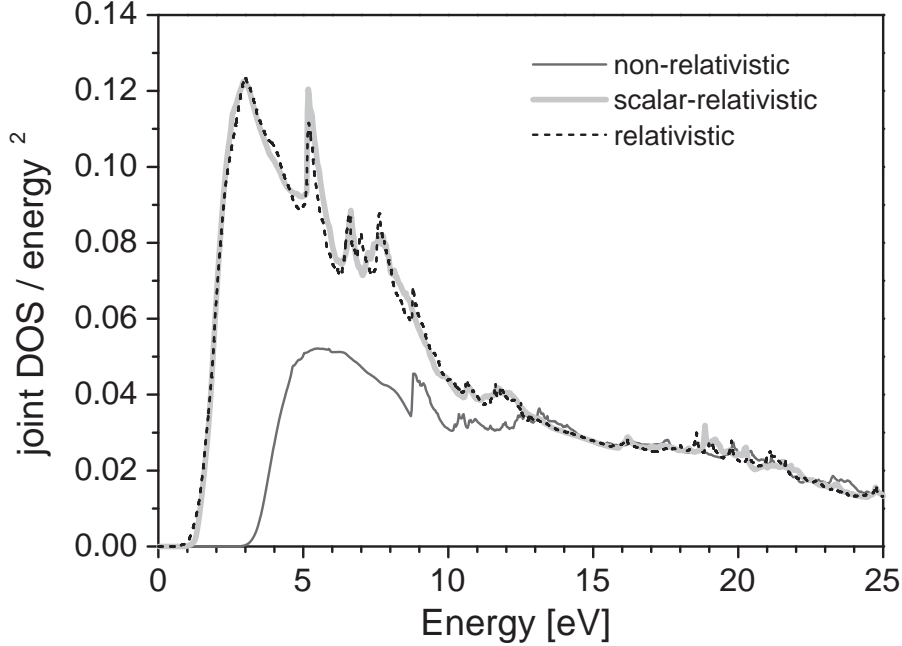


FIG. 7: Joint density of states of gold divided by energy squared. The data are shown for the non-relativistic case (dark gray full line), the scalar-relativistic case (light grey full lines) and the relativistic case (black scattered line).

canceled by selection rules, like the sharp peak at 4.5 eV arising from the parallel bands of d character at -2 eV and s character at 2.5 eV as clearly seen along the line W-L in the BZ. In the non-relativistic case up to 13 eV, the magnitude is much too small and the peaks are found at too high energies as already seen in the optical spectra. Comparing our results to experimental data (Fig. 8), the overall agreement is good. There is two main points which have to be considered. First, the experimental spectrum is in general smaller in magnitude. This seems to be a common problem which can most probably be traced back to a diminished reflectivity at the sample surface.²⁹ Second, although all experimental features are reproduced by theory, the peak positions appear to be slightly too low in the latter. Since most of the transitions contain d states either as initial or as final state, the width of the d band is presumably the source of this shortcoming. The number of effective charges N_{eff} probed by the two sumrules (Eqs.(2.33) and (2.34) behave quite differently as can be seen in Fig. 9. While the integration of $Im\epsilon$ reflects the different magnitudes of theoretical and experimental data, the integration over the loss function is much less sensitive showing very good agreement between theory and experiment in the whole energy range.

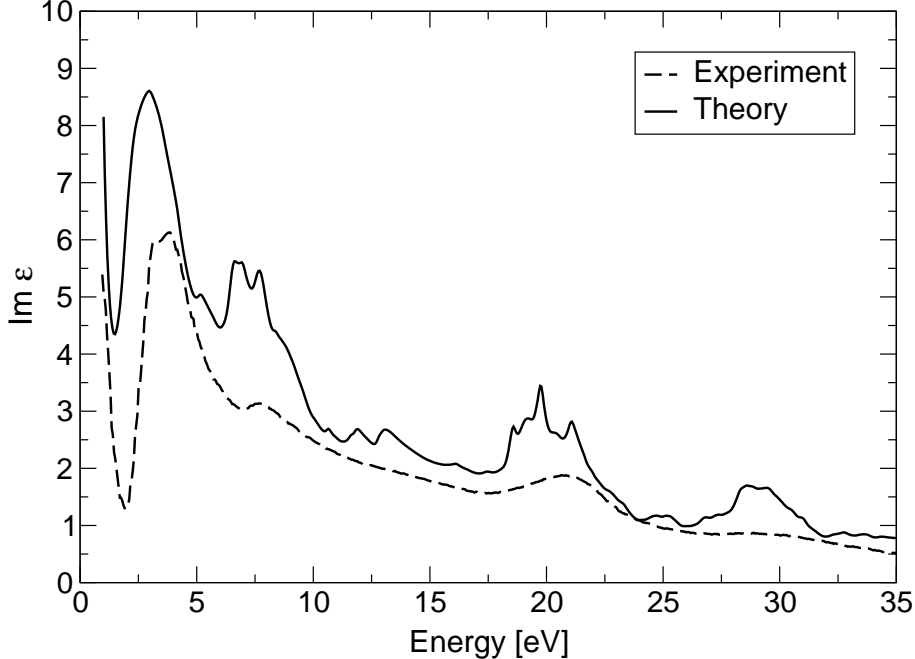


FIG. 8: Imaginary part of the dielectric function for gold including a life-time broadening of 0.1eV obtained by a relativistic calculation compared to the corresponding experiment taken from Cooper et al.²²

Before the over-interpretation of KS states are blamed for the small discrepancies, other reasons should be investigated. From the theoretical side they can be found in the correlation effects being underestimated by the LDA as discussed above, but also in the rather poor basis set of linearized methods for the conduction bands. Furthermore, for the high energy photons the $q = 0$ limit is not justified any more and thus a finite momentum transfer should be considered in future work. But also the experimental side gives rise to shortcomings, as e.g. the Kramers–Kronig analysis requires a continuation of the reflectance spectrum. We need to include $\text{Im } \epsilon$ up to more than 60 eV in the KK transformation in order to obtain $\text{Re } \epsilon$ and henceforth the loss function up to 30 eV reliably.

Although the changes of the band crossing the Fermi level are hardly visible from the band structure, the plasma frequency changes from 9.02 to 9.51 when taking into account scalar-relativistic effects and becomes 8.86 when spin-orbit coupling is introduced. This sensitivity of this quantity is a measure for the reliability of the Fermi surface by the fully-relativistic calculation. ω_{pl} excellently agrees with its experimental counterpart of 8.83.²² An explanation can also be given for the fact that the plasma frequency hardly depends on

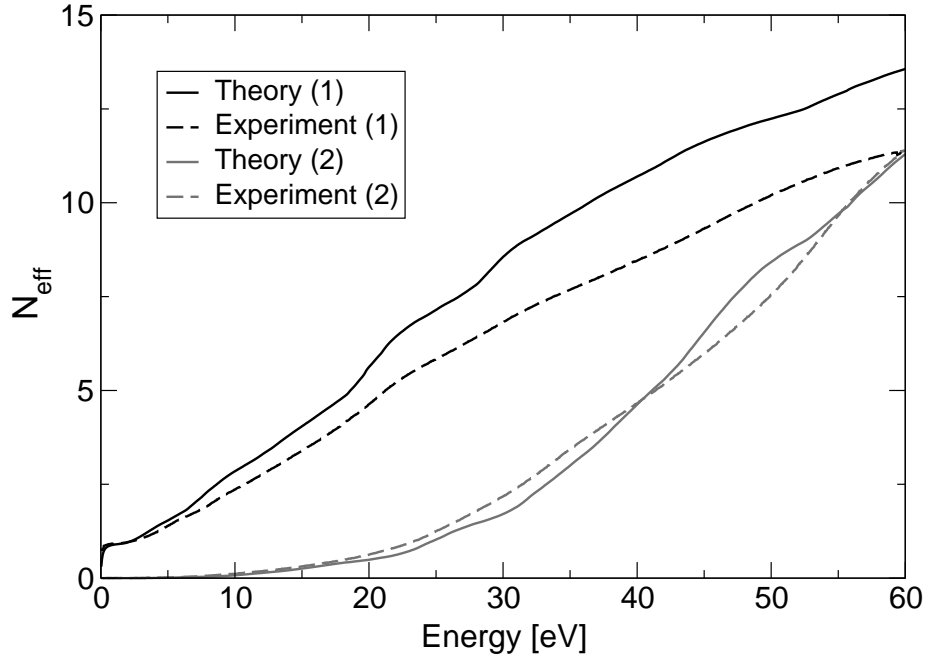


FIG. 9: Sumrule test for the optical spectra of gold obtained by a relativistic calculation compared to the corresponding experiment taken from Cooper et al.²² The numbers in brackets refer to the corresponding sumrules (Eqs. (2.33 and 2.34).

the \mathbf{k} point mesh. Since the only band contributing to the effective number of free carriers has a linear shape around the crossing with the Fermi level the linear tetrahedron method used in our work turns out to be a very effective tool for the Fermi-surface integration.

V. CONCLUSIONS

We have provided a scheme for the calculation of linear optical properties of solids in the random-phase approximation. It is worked out within the LAPW method which does not require approximations in the solution of the KS equation and thus is a good starting point for the evaluation of the KS states in terms of band structure and excited states.

Aluminum, which is a prototype for a free-electron-like metal, exhibits excellent agreement with experiments in terms of plasma frequency, peak positions of the interband transitions, as well as sumrules. This agreement can, however, only be achieved when the BZ integration is carried out with extreme accuracy. Thus highest precision is in general needed to draw conclusions about the quality of the KS states.

For gold, the optical properties are less sensitive to the BZ sampling. The plasma frequency is in excellent agreement with experiment when relativistic effects are taken into account including spin-orbit coupling. The latter is, however, less important for the interband transitions than the scalar-relativistic contributions, i.e. the Darwin shift and the mass-velocity term. Shortcomings can at least be partly traced back to the approximations used for the ground state calculation, i.e. the LDA which does not properly account for correlation effects and thus cannot bring out the d band width and location well enough. Other possible weak points are the insufficient basis set for the unoccupied states, the $q = 0$ limit for high energy transfer, as well as the missing local-field effects. The latter, however, turned out to be of minor importance for the calculation of hot-electron lifetimes.³⁰ All these facts have to be accounted for before a final statement about the interpretability of KS states for a certain material can be made. Nevertheless, in both cases studied here, they provide at least a very good first approximation to single state and excited state energies, respectively.

Acknowledgments

We appreciate support from the Austrian Science Fund (FWF), project P16227-PHY, and by the EU research and training network *EXCITING*, contract number HPRN-CT-2002-00317. The work was supported in part by the Materials Simulation Center, a Penn-State MRSEC and MRI facility.

VI. APPENDIX

A. k.p Perturbation Theory

In the position representation, the one-electron wavefunction $\langle \mathbf{r} | n, \mathbf{k} \rangle = \psi_{n,\mathbf{k}}(\mathbf{r})$ is the solution of the Schrödinger equation

$$\left[\frac{p^2}{2m} + V(\mathbf{r}) \right] \psi_{n,\mathbf{k}}(\mathbf{r}) = \varepsilon_{n,\mathbf{k}} \psi_{n,\mathbf{k}}(\mathbf{r}) . \quad (6.1)$$

Since the crystal potential $V(\mathbf{r})$ has the periodicity of the lattice, using Bloch's theorem we can write

$$\psi_{n,\mathbf{k}}(\mathbf{r}) = e^{i\mathbf{k}\cdot\mathbf{r}} u_{n,\mathbf{k}}(\mathbf{r}) . \quad (6.2)$$

The periodic part of the wavefunction $u_{n,\mathbf{k}}(\mathbf{r})$ obeys

$$H_{\mathbf{k}} u_{n,\mathbf{k}}(\mathbf{r}) = \varepsilon_{n,\mathbf{k}} u_{n,\mathbf{k}}(\mathbf{r}) , \quad (6.3)$$

where

$$H_{\mathbf{k}} = \frac{(\mathbf{p} + \mathbf{k})^2}{2m} + V(\mathbf{r}) . \quad (6.4)$$

We want to obtain an expression for $u_{n,\mathbf{k}+\mathbf{q}}(\mathbf{r})$ and $\varepsilon_{n,\mathbf{k}+\mathbf{q}}$ valid for small \mathbf{q} in terms of the values for $\mathbf{q} = 0$ by perturbation theory. The equation for $u_{n,\mathbf{k}+\mathbf{q}}(\mathbf{r})$ is

$$H_{\mathbf{k}+\mathbf{q}} u_{n,\mathbf{k}+\mathbf{q}}(\mathbf{r}) = \varepsilon_{n,\mathbf{k}+\mathbf{q}} u_{n,\mathbf{k}+\mathbf{q}}(\mathbf{r}) , \quad (6.5)$$

with

$$H_{\mathbf{k}+\mathbf{q}} = H_{\mathbf{k}} + \frac{\hbar \mathbf{p} \cdot \mathbf{q}}{m} + \frac{\hbar^2 \mathbf{k} \cdot \mathbf{q}}{m} + \frac{\hbar^2 q^2}{2m} , \quad (6.6)$$

where the last three terms can be treated as a perturbation.

At this point it will be useful to introduce the notation

$$(\mathbf{r} | n, \mathbf{k}) = u_{n,\mathbf{k}}(\mathbf{r}) \quad (6.7)$$

and

$$\left(n', \mathbf{k}' | \hat{O} | n, \mathbf{k} \right) = \frac{1}{\Omega} \int_{\Omega} d\mathbf{r} u_{n',\mathbf{k}'}^*(\mathbf{r}) \hat{O} u_{n,\mathbf{k}}(\mathbf{r}) , \quad (6.8)$$

for any operator \hat{O} with the integral running over the unit cell of volume Ω .

According to this notation, the wavefunction to first order in \mathbf{q} for a non-degenerate state is

$$|n, \mathbf{k} + \mathbf{q}\rangle = |n, \mathbf{k}\rangle + \sum_{n' \neq n} |n', \mathbf{k}\rangle \frac{(n', \mathbf{k} | H_{\mathbf{k}+\mathbf{q}} - H_{\mathbf{k}} | n, \mathbf{k})}{\varepsilon_{n,\mathbf{k}} - \varepsilon_{n',\mathbf{k}}} \quad (6.9)$$

Only one term from the perturbation Hamiltonian gives a contribution different from zero to the first order correction of the wavefunction

$$|n, \mathbf{k} + \mathbf{q}\rangle = |n, \mathbf{k}\rangle + \sum_{n' \neq n} |n', \mathbf{k}\rangle \frac{(n', \mathbf{k} | \frac{\hbar}{m} \mathbf{p} \cdot \mathbf{q} | n, \mathbf{k})}{\varepsilon_{n,\mathbf{k}} - \varepsilon_{n',\mathbf{k}}} \quad (6.10)$$

To linear order in \mathbf{q} the expression for the energy is

$$\varepsilon_{n,\mathbf{k}+\mathbf{q}} = \varepsilon_{n,\mathbf{k}} + \left(n, \mathbf{k} \left| \frac{\hbar \mathbf{p} \cdot \mathbf{q}}{m} + \frac{\hbar^2 \mathbf{k} \cdot \mathbf{q}}{m} \right| n, \mathbf{k} \right) . \quad (6.11)$$

Since the states are normalized this expression can be written as

$$\varepsilon_{n,\mathbf{k}+\mathbf{q}} = \varepsilon_{n,\mathbf{k}} + \frac{\hbar}{m} [(n, \mathbf{k} | \mathbf{p} | n, \mathbf{k}) + \hbar \mathbf{k}] \cdot \mathbf{q} \quad (6.12)$$

The momentum matrix element evaluated in Section III B can be expressed as

$$\mathbf{p}_{l,n,\mathbf{k}} \equiv \langle l, \mathbf{k} | \mathbf{p} | n, \mathbf{k} \rangle = \delta_{l,n} \hbar \mathbf{k} + (l, \mathbf{k} | \mathbf{p} | n, \mathbf{k}) . \quad (6.13)$$

In terms of this definition, the wavefunctions and energies to first order in \mathbf{q} are given by

$$|n, \mathbf{k} + \mathbf{q}\rangle = |n, \mathbf{k}\rangle + \frac{\hbar}{m} \sum_{n' \neq n} |n', \mathbf{k}\rangle \frac{\mathbf{P}_{n',n,\mathbf{k}}}{\varepsilon_{n,\mathbf{k}} - \varepsilon_{n',\mathbf{k}}} \cdot \mathbf{q} \quad (6.14)$$

and

$$\varepsilon_{n,\mathbf{k}+\mathbf{q}} = \varepsilon_{n,\mathbf{k}} + \frac{\hbar}{m} \mathbf{P}_{n,n,\mathbf{k}} \cdot \mathbf{q} \quad (6.15)$$

B. Matrix elements for small q

In this appendix we use the $\mathbf{k} \cdot \mathbf{p}$ expressions developed in Appendix VI A to evaluate the matrix elements for $\mathbf{q} \rightarrow 0$. We first write the matrix elements in terms of the periodic part of the wavefunction

$$M_{l,n}^0(\mathbf{k}, \mathbf{q}) = \langle l, \mathbf{k} | e^{-i\mathbf{q}\cdot\mathbf{r}} | n, \mathbf{k} + \mathbf{q} \rangle = (l, \mathbf{k} | n, \mathbf{k} + \mathbf{q}) . \quad (6.16)$$

Using the expression of the wavefunction for small \mathbf{q} of Eq.(6.14), the matrix element at lowest order is

$$M_{l,n}^0(\mathbf{k}, \mathbf{q} \rightarrow 0) = \delta_{l,n} + (1 - \delta_{l,n}) \frac{\hbar}{m} \frac{\mathbf{P}_{l,n,\mathbf{k}}}{\varepsilon_{n,\mathbf{k}} - \varepsilon_{l,\mathbf{k}}} \cdot \mathbf{q} \quad (6.17)$$

C. Relations between spherical harmonics

Below, several well known relations between the spherical harmonics are given, which are needed to evaluate the momentum matrix elements:

$$e^{+i\varphi} \sin \theta Y_{l,m} = F_{l,m}^{(1)} Y_{l+1,m+1} + F_{l,m}^{(2)} Y_{l-1,m+1} \quad (6.18)$$

$$e^{-i\varphi} \sin \theta Y_{l,m} = F_{l,m}^{(3)} Y_{l+1,m-1} + F_{l,m}^{(4)} Y_{l-1,m-1} \quad (6.19)$$

$$\cos \theta Y_{l,m} = F_{l,m}^{(5)} Y_{l+1,m} + F_{l,m}^{(6)} Y_{l-1,m} \quad (6.20)$$

with

$$F_{l,m}^{(1)} = - \sqrt{\frac{(l+m+1)(l+m+2)}{(2l+1)(2l+3)}} \quad (6.21)$$

$$F_{l,m}^{(2)} = \sqrt{\frac{(l-m)(l-m-1)}{(2l-1)(2l+1)}} \quad (6.22)$$

$$F_{l,m}^{(3)} = \sqrt{\frac{(l-m+1)(l-m+2)}{(2l+1)(2l+3)}} \quad (6.23)$$

$$F_{l,m}^{(4)} = - \sqrt{\frac{(l+m)(l+m-1)}{(2l-1)(2l+1)}} \quad (6.24)$$

$$F_{l,m}^{(5)} = \sqrt{\frac{(l-m+1)(l+m+1)}{(2l+1)(2l+3)}} \quad (6.25)$$

$$F_{l,m}^{(6)} = \sqrt{\frac{(l-m)(l+m)}{(2l-1)(2l+1)}} \quad (6.26)$$

$$e^{+i\varphi} \left(\cos \theta \frac{\partial}{\partial \theta} + \frac{i}{\sin \theta} \frac{\partial}{\partial \varphi} \right) Y_{l,m} = -l F_{l,m}^{(1)} Y_{l+1,m+1} + (l+1) F_{l,m}^{(2)} Y_{l-1,m+1} \quad (6.27)$$

$$e^{-i\varphi} \left(\cos \theta \frac{\partial}{\partial \theta} - \frac{i}{\sin \theta} \frac{\partial}{\partial \varphi} \right) Y_{l,m} = -l F_{l,m}^{(3)} Y_{l+1,m-1} + (l+1) F_{l,m}^{(4)} Y_{l-1,m-1} \quad (6.28)$$

$$- \sin \theta \frac{\partial}{\partial \theta} Y_{l,m} = -l F_{l,m}^{(5)} Y_{l+1,m+1} + (l+1) F_{l,m}^{(6)} Y_{l-1,m+1} \quad (6.29)$$

D. The step function

The analytic evaluation of a planewave integral over the interstitial region as needed in Eq. (3.28) is carried out by integrating over the whole unit cell and subtracting the contributions of the atomic spheres, which are

$$\int_{MT_\alpha} e^{i(\mathbf{G}'-\mathbf{G})\mathbf{r}} d\mathbf{r} = \begin{cases} V_\alpha & \mathbf{G}' = \mathbf{G} \\ 3V_\alpha \frac{\sin(R_\alpha|\mathbf{G}'-\mathbf{G}|) - \cos(R_\alpha|\mathbf{G}'-\mathbf{G}|)}{(R_\alpha|\mathbf{G}'-\mathbf{G}|)^3} e^{i(\mathbf{G}'-\mathbf{G})\mathbf{S}_\alpha} & \mathbf{G}' \neq \mathbf{G} \end{cases} \quad (6.30)$$

It utilizes the Rayleigh-expansion of a planewave in terms of spherical harmonics:

$$e^{i\mathbf{G}\mathbf{r}} = 4\pi e^{i\mathbf{G}\mathbf{S}_\alpha} \sum_{lm} i^l j_l(|\mathbf{r}-\mathbf{S}_\alpha|G) Y_{lm}^*(\hat{\mathbf{G}}) Y_{lm}(\widehat{\mathbf{r}-\mathbf{S}_\alpha}). \quad (6.31)$$

E. Local orbitals

The extension of the LAPW basis set by localized orbitals¹⁵ was introduced in order to describe semi-core states, i.e. those low-lying states which reach out of the atomic sphere, on the same footing as valence states. The corresponding basis functions reads inside the atomic sphere

$$\begin{aligned} \phi_{\mathbf{k},lm}^{LO}(\mathbf{S}_\alpha + \mathbf{r}) = \\ [A_{lm}^\alpha(\mathbf{k} + \mathbf{G}_{lm}^{LO})u_l^\alpha(r, E_l) + B_{lm}^\alpha(\mathbf{k} + \mathbf{G}_{lm}^{LO})\dot{u}_l^\alpha(r, E_l) + C_{lm}^\alpha(\mathbf{k} + \mathbf{G}_{lm}^{LO})u_l^\alpha(r, E_l^{LO})] Y_{l,m}(\hat{\mathbf{r}}) \end{aligned} \quad (6.32)$$

and is zero outside. The coefficients $A_{lm}^\alpha(\mathbf{k} + \mathbf{G}_l^{LO})$, $B_{lm}^\alpha(\mathbf{k} + \mathbf{G}_l^{LO})$, and $C_{lm}^\alpha(\mathbf{k} + \mathbf{G}_l^{LO})$ are determined by choosing $\phi_{\mathbf{k},lm}^{LO}$ and its spatial derivative to vanish at the sphere boundary, and by the normalization condition for $\phi_{\mathbf{k},lm}^{LO}$. The additional trial energy E_l^{LO} corresponds to the energy of the semi-core state, and for each localized basis function one specific \mathbf{G}_{lm}^{LO} is chosen.¹⁵ The wavefunction can then be written as

$$\Psi_{n\mathbf{k}}(\mathbf{r}) = \sum_{\mathbf{G}} C_{n\mathbf{k}}(\mathbf{G})\phi_{\mathbf{k}+\mathbf{G}}(\mathbf{r}) + \sum_{lm} C_{n\mathbf{k},lm}^{LO}(\mathbf{G}_{lm}^{LO})\phi_{\mathbf{k},lm}^{LO}(\mathbf{r}) \quad (6.33)$$

Analogously to Eqs. (3.14–3.16) matrix elements between LAPW's and LO's

$${}^\alpha\Phi_{\mathbf{k}l m, \mathbf{k}+\mathbf{G}}^{x+iy} \equiv \langle \phi_{\mathbf{k},lm}^{LO}(\mathbf{S}_\alpha + \mathbf{r}) | \partial x + i\partial y | \phi_{\mathbf{k}+\mathbf{G}}(\mathbf{S}_\alpha + \mathbf{r}) \rangle \quad (6.34)$$

$${}^\alpha\Phi_{\mathbf{k}l m, \mathbf{k}+\mathbf{G}}^{x-iy} \equiv \langle \phi_{\mathbf{k},lm}^{LO}(\mathbf{S}_\alpha + \mathbf{r}) | \partial x - i\partial y | \phi_{\mathbf{k}+\mathbf{G}}(\mathbf{S}_\alpha + \mathbf{r}) \rangle \quad (6.35)$$

$${}^\alpha\Phi_{\mathbf{k}l m, \mathbf{k}+\mathbf{G}}^z \equiv \langle \phi_{\mathbf{k},lm}^{LO}(\mathbf{S}_\alpha + \mathbf{r}) | \partial z | \phi_{\mathbf{k}+\mathbf{G}}(\mathbf{S}_\alpha + \mathbf{r}) \rangle \quad (6.36)$$

and between LO's and LO's have to be defined:

$${}^\alpha\Phi_{\mathbf{k}l'm', \mathbf{k}lm}^{x+iy} \equiv \langle \phi_{\mathbf{k},l'm'}^{LO}(\mathbf{S}_\alpha + \mathbf{r}) | \partial x + i\partial y | \phi_{\mathbf{k},lm}^{LO}(\mathbf{S}_\alpha + \mathbf{r}) \rangle \quad (6.37)$$

$${}^\alpha\Phi_{\mathbf{k}l'm', \mathbf{k}lm}^{x-iy} \equiv \langle \phi_{\mathbf{k},l'm'}^{LO}(\mathbf{S}_\alpha + \mathbf{r}) | \partial x - i\partial y | \phi_{\mathbf{k},lm}^{LO}(\mathbf{S}_\alpha + \mathbf{r}) \rangle \quad (6.38)$$

$${}^\alpha\Phi_{\mathbf{k}l'm', \mathbf{k}lm}^z \equiv \langle \phi_{\mathbf{k},l'm'}^{LO}(\mathbf{S}_\alpha + \mathbf{r}) | \partial z | \phi_{\mathbf{k},lm}^{LO}(\mathbf{S}_\alpha + \mathbf{r}) \rangle \quad (6.39)$$

The atomic sphere parts of the momentum matrix elements given in Eq. (3.27) have to be supplemented by contributions from the local orbitals:

$$\begin{aligned}
\langle n'\mathbf{k} | \nabla_x | n\mathbf{k} \rangle_{\text{MT}\alpha} &= \frac{1}{2} \sum_{G',G} C_{n'\mathbf{k}}^*(\mathbf{G}') (\alpha \Phi_{\mathbf{k}+\mathbf{G}',\mathbf{k}+\mathbf{G}}^{x+iy} + \alpha \Phi_{\mathbf{k}+\mathbf{G}',\mathbf{k}+\mathbf{G}}^{x-iy}) C_{n\mathbf{k}}(\mathbf{G}) \\
&+ \frac{1}{2} \sum_{lm,G} C_{n'\mathbf{k},lm}^{*LO}(\mathbf{G}_{lm}^{LO}) (\alpha \Phi_{\mathbf{k}l\mathbf{m},\mathbf{k}+\mathbf{G}}^{x+iy} + \alpha \Phi_{\mathbf{k}l\mathbf{m},\mathbf{k}+\mathbf{G}}^{x-iy}) C_{n\mathbf{k}}(\mathbf{G}) \\
&+ \frac{1}{2} \sum_{l'm',lm} C_{n'\mathbf{k},l'm'}^{*LO}(\mathbf{G}_{l'm'}^{LO}) (\alpha \Phi_{\mathbf{k}l'm',\mathbf{k}l\mathbf{m}}^{x+iy} + \alpha \Phi_{\mathbf{k}l'm',\mathbf{k}l\mathbf{m}}^{x-iy}) C_{n\mathbf{k},lm}^{LO}(\mathbf{G}_{lm}^{LO})
\end{aligned} \tag{6.40}$$

$$\begin{aligned}
\langle n'\mathbf{k} | \nabla_y | n\mathbf{k} \rangle_{\text{MT}\alpha} &= \frac{1}{2i} \sum_{G',G} C_{n'\mathbf{k}}^*(\mathbf{G}') (\alpha \Phi_{\mathbf{k}+\mathbf{G}',\mathbf{k}+\mathbf{G}}^{x+iy} - \alpha \Phi_{\mathbf{k}+\mathbf{G}',\mathbf{k}+\mathbf{G}}^{x-iy}) C_{n\mathbf{k}}(\mathbf{G}) \\
&+ \frac{1}{2i} \sum_{lm,G} C_{n'\mathbf{k},lm}^{*LO}(\mathbf{G}_{lm}^{LO}) (\alpha \Phi_{\mathbf{k}l\mathbf{m},\mathbf{k}+\mathbf{G}}^{x+iy} - \alpha \Phi_{\mathbf{k}l\mathbf{m},\mathbf{k}+\mathbf{G}}^{x-iy}) C_{n\mathbf{k}}(\mathbf{G}) \\
&+ \frac{1}{2i} \sum_{l'm',lm} C_{n'\mathbf{k},l'm'}^{*LO}(\mathbf{G}_{l'm'}^{LO}) (\alpha \Phi_{\mathbf{k}l'm',\mathbf{k}l\mathbf{m}}^{x+iy} - \alpha \Phi_{\mathbf{k}l'm',\mathbf{k}l\mathbf{m}}^{x-iy}) C_{n\mathbf{k},lm}^{LO}(\mathbf{G}_{lm}^{LO})
\end{aligned} \tag{6.41}$$

$$\begin{aligned}
\langle n'\mathbf{k} | \nabla_z | n\mathbf{k} \rangle_{\text{MT}\alpha} &= \sum_{G',G} C_{n'\mathbf{k}}^*(\mathbf{G}') \alpha \Phi_{\mathbf{k}+\mathbf{G}',\mathbf{k}+\mathbf{G}}^z C_{n\mathbf{k}}(\mathbf{G}) \\
&+ \sum_{lm,G} C_{n'\mathbf{k},lm}^{*LO}(\mathbf{G}_{lm}^{LO}) \alpha \Phi_{\mathbf{k}l\mathbf{m},\mathbf{k}+\mathbf{G}}^z C_{n\mathbf{k}}(\mathbf{G}) \\
&+ \sum_{l'm',lm} C_{n'\mathbf{k},l'm'}^{*LO}(\mathbf{G}_{l'm'}^{LO}) \alpha \Phi_{\mathbf{k}l'm',\mathbf{k}l\mathbf{m}}^z C_{n\mathbf{k},lm}^{LO}(\mathbf{G}_{lm}^{LO})
\end{aligned} \tag{6.42}$$

The evaluation of Eqs. (6.34-6.39) is straightforward analogous to Eqs. (3.24-3.26).

¹ P. Hohenberg and W. Kohn, Phys. Rev. **136**, B 864 (1964).

² W. Kohn and L. J. Sham, Phys. Rev. **140**, A 1133 (1965).

³ M. S. Hybertsen and S. G. Louie, Phys. Rev. B **34**, 5390 (1986).

⁴ Z. H. Levine, D. C. Allan, *Phys. Rev. Lett.* **63**, 1719 (1989), Z. H. Levine, D.C. Allan, *Phys. Rev. B* **43**, 4187 (1991).

⁵ Neil W. Ashcroft and N. David Mermin, *Solid State Physics*, (Saunders College Publishing, Fort Worth, TX, U.S.A., 1976) p.344.

⁶ S. L. Adler, Phys. Rev. **126**, 413 (1962).

⁷ N. Wiser, Phys. Rev. **129**, 62 (1963).

- ⁸ L. Hedin, Phys. Rev. **139**, A796 (1965).
- ⁹ L. P. Kadanoff and G. Baym, *Quantum Statistical Mechanics*, (Addison Wesley, New York, 1989).
- ¹⁰ N. Vast, L. Reining, V. Olevano, P. Schattschneider, and B. Jouffrey, Phys. Rev. Lett. **88**, 037601 (2002) and Refs. therein.
- ¹¹ O. K. Andersen, Phys. Rev. B **12**, 3060 (1975).
- ¹² D. Singh, Planewaves, *Pseudopotentials and the LAPW Method* (Kluwer Academic Publishers, Boston, Dordrecht, London, 1994).
- ¹³ R. Abt, PhD Thesis, University of Graz, 1997.
- ¹⁴ P. Blaha, K. Schwarz, and J. Luitz, *WIEN97, A Full Potential Linearized Augmented Plane Wave Package for Calculating Crystal Properties*, Technische Universität Wien, Austria, 1999, ISBN 3-9501031-0-4.
- ¹⁵ D. Singh, Phys. Rev. B **43**, 6388 (1991).
- ¹⁶ H. Ehrenreich, H. R. Philipp, and B. Segall, Phys. Rev. **132**, 1918 (1963).
- ¹⁷ E. Shiles, T. Sasaki, M. Inokuti, and D. Y. Smith, Phys. Rev. B **22**, 1612 (1980).
- ¹⁸ F. Szmulowicz and B. Segall, Phys. Rev. B **24**, 892 (1981).
- ¹⁹ D. Y. Smith and B. Segall, Phys. Rev. B **34**, 5191 (1986).
- ²⁰ K.-H. Lee and K. J. Chang, Phys. Rev. B **49**, 2362 (1994).
- ²¹ This problem was avoided in Ref. 18 by using a $\mathbf{k}\cdot\mathbf{p}$ interpolation for the APW results.
- ²² B. R. Cooper, H. Ehrenreich, and H. R. Philipp, Phys. Rev. **138**, A494 (1965).
- ²³ P. B. Johnson and R. W. Christy, Phys. Rev. B **6**, 4370 (1972).
- ²⁴ N. E. Christensen and B. O. Seraphin, Phys. Rev. B **4**, 3321 (1971) and references therein.
- ²⁵ N. E. Christensen, Phys. Rev. B **13**, 2698 (1976).
- ²⁶ T. Takeda, J. Phys. F: Metal Phys. **10**, 1135 (1980).
- ²⁷ V. Theileis and H. Bross, Phys. Rev. B **62**, 13338 (2000) and references therein.
- ²⁸ R. Lässer, N. V. Smith, and R. L. Benbow, Phys. Rev. B **24**, 1895 (1981).
- ²⁹ K. Glantschnig and C. Ambrosch-Draxl, submitted to Phys. Rev. B
- ³⁰ F. Ladstädter, P. F. de Pablos, U. Hohenester, P. Puschnig, C. Ambrosch-Draxl, P. L. de Andres, F.-J. Garcia-Vidal, and F. Flores, Phys. Rev. B **68**, 085107 (2003).